Energy-Based Fatigue Life Prediction Under Random Uniaxial and Multiaxial Loadings

by

Shih-Chuan Tien

A Thesis Presented in Partial Fulfillment
of the Requirement for the Degree
Master of Science

Approved April 2021 by the
Graduate Supervisory Committee:

Yongming Liu, Chair
Qiong Nian
Yang Jiao

ARIZONA STATE UNIVERSITY

May 2021

ABSTRACT

Two fatigue life prediction methods using the energy-based approach have been proposed. A number of approaches have been developed in the past five decades. This study reviews some common models and discusses the model that is most suitable for each different condition, no matter whether the model is designed to solve uniaxial, multiaxial, or biaxial loading paths in fatigue prediction. In addition, different loading cases such as various loading and constant loading are also discussed. These models are suitable for one or two conditions in fatigue prediction. While most of the existing models can only solve single cases, the proposed new energy-based approach not only can deal with different loading paths but is applicable for various loading cases. The first energy-based model using the linear cumulative rule is developed to calculate random loading cases. The method is developed by combining Miner's rule and the rainflow-counting algorithm. For the second energy-based method, I propose an alternative method and develop an approach to avert the rainflow-counting algorithm. Specifically, I propose to use an energy-based model by directly using the time integration concept. In this study, first, the equivalent energy concept that can transform three-dimensional loading into an equivalent loading will be discussed. Second, the new damage propagation method modified by fatigue crack growth will be introduced to deal with cycle-based fatigue prediction. Third, the time-based concept will be implemented to determine fatigue damage under every cycle in the random loading case. The formulation will also be explained in detail. Through this new model, the fatigue life can be calculated properly in different loading cases. In addition, the proposed model is verified with experimental datasets from several published studies. The data include both uniaxial and multiaxial loading paths under constant loading and random loading cases. Finally, the discussion and conclusion based on the results, are included. Additional loading cases such as the spectrum including both elastic and plastic regions will be explored in future research.

DEDICATION

To my parents and family for their endless support. To Dr. Tein, my aunt, who encourages me to step out of my comfort zone. She is the best mentor in the world.

ACKNOWLEDGMENTS

I would like to express my sincere gratitude to my advisor, Dr. Yongming Liu for his continuous support and guidance of my master's thesis. Through his motivation, enthusiasm, and immense expertise, I have gained tremendous knowledge in fatigue for the last two years. I appreciate Dr. Qiong Nian and Dr. Yang Jiao before being my committee members and for their support. I would also like to thank Haoyang Wei who has patiently taught me not only fatigue, but knowledge beyond classwork and the textbook.

TABLE OF CONTENTS

Page

LIST OF TABLES iv

LIST OF FIGURES v

CHAPTER

1 INTRODUCTION 1

2 ENERGY-BASED FATIGUE MODEL USING THE LINEAR CUMULATIVE DAMAGE RULE 6

2.1 Equivalent Energy Concept 6

2.2 Application of Linear Cumulative Damage Rule and Rainflow-counting Algorithm 7

2.3 Model Energy Using Linear Cumulative Damage Rule 8

2.4 Validation 10

2.5 Conclusion 10

3 TIME-BASED FATIGUE LIFE PREDICTION MODEL USING ENERGY-BASED METHOD 12

3.1 Damage Propagation Based on Paris' Law Development 13

3.2 Sub-cycle Damage Growth Function Development 18

3.3 Model Parameter Calibration 24

3.4 Model Validation 26

4 SUMMARY 42

REFERENCES 44

Page

A SPECTRUM TRANSFER 48

B TIME-BASED FATIGUE MODEL FOR CONSTANT LOADING CASE 52

C TIME-BASED FATIGUE MODEL FOR RANDOM LOADING CASE 59

LIST OF TABLES

Table Page

Table 1. Summary of Fatigue Testing Spectrum under Random Loading Conditions in HCF. 27

Table 2. Summary of Fatigue Testing Spectrum under Random Loading Conditions in HCF+LCF. 27

Table 3. Summary of Collected Experimental Data. 28

LIST OF FIGURES

Figure Page

Fig. 1 Comparison Between Predicted and Experimental Fatigue Life Under Al T7075 ..10

Fig. 2 Time-based Fatigue Model Flow-Chart 12

Fig. 3 Time-Based Integration Concept 13

Fig. 4 The Relationship Between Crack Length Growth Rate and Stress Intensity Range in Log Scale 14

Fig. 5 Stress Spectrum 16

Fig. 6 Energy Spectrum 17

Fig. 7 The Relationship of Crack Length Increase Rate and CTOD at Sub-Cycle Scale [27] 19

Fig. 8 Stress Paths of Data Used in the Current Study..... 28

Fig. 9 Generated Spectrum for Fatigue Testing Under Multiaxial Random Loading..... 31

Fig. 10 Generated Spectrum for Fatigue Testing Under Uniaxial Random Loading..... 32

Fig. 11 HCF+LCF Spectrum for Fatigue Testing Under Multiaxial Random Loading..... 34

Fig. 12 Predicted Fatigue Life and Experimental Fatigue Life Comparison in Constant Loading Case: (a) AISI 304 Steel (b) SM45C Steel (c) A533B (d) S460N (e) SAE 1045 (f) Al T6061 (g) Al T7075..... 38

Fig. 13 Predicted Fatigue Life and Experimental Fatigue Life Comparison in Random Loading Case for Aluminium T7075 39

Fig. 14 The Predicted Fatigue Life in Different Sampling Rate 40

CHAPTER 1

1 INTRODUCTION

Fatigue is a critical issue that has been researched for many years. Most failures or fractures in materials have been caused by fatigue. Fatigue can be classified into several types according to different loading paths, such as uniaxial fatigue, multiaxial fatigue, and biaxial fatigue. Multiaxial fatigue can be found in mechanical components and it is the most common phenomenon. Accurate prediction of fatigue life is very important to ensure the life span of any structural component used in the real world. Research on fatigue has been conducted over the past half century and several related methods have been proposed. The main categories of the methods are stress-based [1–3], strain-based [4–6], energy-based [7–10], and fracture mechanics-based [11,12], other methods [13,14]. These methods were developed to predict fatigue life in different perspectives.

The stress-based approach is a popular method used to predict the fatigue life cycle, especially in high cycle fatigue (HCF). For example, the stress-based model, proposed by Liu and colleagues [15], modified the critical plane approach to develop a new criterion for predicting fatigue life in multiaxial states in constant loading. Another stress-based approach, proposed by Wei and colleagues [2], extended the modified critical plane [15] by combining the rainflow-counting algorithm and Miner's rule to develop a new model suitable for predicting fatigue life in random loading cases. Also, other stress-based approaches have been proposed to use different high-cycle fatigue criteria to predict in-phase and out-of-phase multiaxial fatigue [16–18]. However, this stress-based model has a drawback such that the model is not suitable to deal with plastic regions experiencing low cycle fatigue (LCF). When the material deformation approaches, the plastic region it leads the relationship between strain and stress from linear to nonlinear, therefore the relationship between stress and strain cannot be defined correctly in HCF. Moreover, the

stress-strain curve in the plastic region is nonproportional and very unpredictable. Thus, the strain-based approach was developed to overcome this situation.

The strain-based approach is proposed by several authors based on different concepts. For example, a strain-based model proposed by Liu [4], is based on a characteristic plane which is a modified critical plan concept and can deal with multiaxial loading condition well. Another strain-based model for fatigue crack method, proposed by Remes [5], can predict the fatigue life of a notch shape for a welded steel joint. Many strain-based models are proposed to handle specific engineering problems. Even though the strain-based models can deal with the LCF, some special cases, such as perfectly elastic material, cannot be solved by this approach. Since the strain-based method is only related to strain, the out-of-phase hardening phenomenon would need another technique.

To predict both HCF and LCF fatigue life, the energy-based approach is proposed [8–10,19,20]. It can solve the stress-based and strain-based model issues dealing with HCF and LCF in different loading conditions, at the same time. The energy-based approach includes both the stress and strain in the model so that it can cope with broad situations. The energy-based approach can directly use Young's modulus to acquire stress or strain in HCF. However, the relationship between stress and strain in the plastic region needs to be solved by additional models, such as the models proposed by Garud and Mróz [21,22] which can deal with the plasticity and determine the stress-strain curve in the plastic region. Even though the energy-based approach seems to be a very powerful method, the energy concept cannot be directly observed by eyes in physical phenomenon. On the other hand, the energy-based approach takes stress and strain into account and can include more conditions than other methods. Therefore, the energy-based model has been chosen in this study.

Beyond the three main classifications above, there are a few different approaches to predict fatigue life. The fracture mechanics-based approach uses the crack growth and the equivalent initial flaw size (EIFS) concept for the crack growth model in the Kitagawa Takahashi diagram. The detail about this method can be found in [23]. The fatigue model with the EIFS concept is also suitable for uniaxial and multiaxial loading cases [23,24]. The different loading can be found in the mechanical component structure. The loading spectrum can be classified into two types, constant loading and various (or random) loading. Multiaxial constant loading has been predicted very well by several models such as [1,4,9,15]. These models are proposed to predict constant loading since random loading is a more complex condition and involves other relative methods such as the rainflow-counting algorithm. In general, the various loading spectrum condition includes various waves and a different R ratio in every cycle so that the prediction can be influenced by the R ratio, which means that the cyclic loading has different mean stress and is more difficult to model in a complicated random loading condition. As a result, several models are designed to overcome this conundrum. For the random loading multiaxial fatigue study there is one review paper that summarizes several criterions for solving random loading cases [25]. This review includes many definitions for different methods. For example, the fatigue model under a various loading spectrum can classify in two domains, time or frequency. Also, different damage rules are chosen under different models. The damage rule can be classified as linear and nonlinear.

In existing literature studies there was no method suitable for both HCF and LCF as well as for constant loading and random loading cases. Moreover, the existing models apply complicated criterions to solve the problem such that different stress ratios exist in different cycles. This study is inspired by a desire to build a model that simplifies the complex procedure while at the same time predicting fatigue life in several conditions. The

new idea will develop a model that is suitable for constant and various loading but also can deal with the HCF and LCF conditions.

In view of this, the energy-based model using the linear damage accumulation rule is proposed initially. The equivalent energy concept which is applied to this method combines the rainflow-counting algorithm and the damage accumulated rule to predict fatigue life. However, this method cannot properly obtain fatigue life prediction since the equivalent energy after applying rainflow-counting algorithm cannot track the spectrum history well. The author seeks an alternative way to curtail the process and make the predicted process clearer. Therefore, a more comprehensive approach, a time-based multiaxial fatigue prediction model using the energy-based method is proposed. In the past, the random loading fatigue model used the rainflow-counting algorithm to simplify the complex wave spectrum in order to acquire equivalent stress or strain. In this study, the rainflow-counting algorithm is removed and replaced by using a clear integration method. This method applies the time-based concept [26,27] to gather corresponding damage with energy under every cycle. The approach integrates the equivalent energy concept, crack propagation, and time-based concept to solve the random loading issue while being suitable for both HCF and LCF conditions. In this method, the crack propagation concept is modified to correspond to a new damage propagation concept. First, through the equivalent energy concept, the energy can be classified into two energies, distortional and dilatational energy. This simplified process can solve multiaxial loading easily. Secondly, the accumulation of damage per cycle can be solved by using damage propagation to calculate fatigue life in a cycle-based method. Lastly, the time-based concept is introduced to calculate the damage accumulation in a cycle. This concept can predict various models with no need to use the rainflow-counting algorithm.

The rest of the thesis will have the following arrangement. The equivalent energy concept will be reviewed with the energy-based model using the linear damage accumulated rule being discussed in detail in Chapter Two. The time-based model will be introduced in Chapter Three. The model will be introduced in Chapter Three where the damage propagation concept which modified by crack growth rule will be described in detail initially. Then, the time-based concept using in time-based model will be introduced. In addition, the validation of the model using several databases from existing documents will be presented. Finally, a conclusion and discussion of the results will be presented in Chapter Four. The future work also is mentioned at the end.

CHAPTER 2

2 ENERGY-BASED FATIGUE MODEL USING THE LINEAR CUMULATIVE DAMAGE RULE

2.1 Equivalent Energy Concept

The equivalent energy concept was proposed by Wei [9]. The material under the HCF loading can be predicted properly by using the stress-based method. However, the stress-based method cannot predict the condition when a material approaches the plastic region since the strain growth is not proportional to stress. On the other hand, the strain-based method is more suitable for LCF fatigue prediction. However, the strain-based method is highly sensitive with experimental data. The energy-based method takes both stress and strain into account so that the method can be applied to more conditions. Under the energy-based model, the stress and strain history needs to be transfered to energy history. In the fatigue life prediction research, energy is classified under two major components, dilatational and distortional energy, which is calculated under three-dimensional conditions. The dilatational energy represents the volume change, and the distortional energy represents the shape change in the material. The two energy components are used in the proposed energy damage parameters. The equivalent tensile energy, torsional energy, and hydrostatic energy are used under failure damage criterion and are related to experimental data which are obtained from uniaxial and pure torsional fatigue life data. Under this concept, general energy (total energy) can be decomposed to dilatational and distortional energy, as shown below.

$$U_{total} = U_{dil} + U_{dis} \tag{2.1}$$

where U_{total} is the total energy, U_{dil} is dilatational energy, and U_{dis} is distortional energy. Both dilatational and distortional energy can be classified under three other energy terms, tensile, torsional, or hydrostatic energy. The whole derivative process which calculates

from input dilatational and distortional energy to the three energy terms to output to equivalent energy is not shown here. Only the final equation is mentioned here. The equation can be expressed as

$$U_{ten}^{eq} = U_{ten} + sU_{tor} + kU_H \quad (2.2)$$

where U_{ten}^{eq} is equivalent energy, U_{ten} is tensile energy, U_{tor} is torsional energy, U_H is hydrostatic energy, s is a ratio of tensile and torsional fatigue limit, and k is a material parameter related to yield-to-ultimate strength ratio and Poisson' ratio. A detailed description of the method can be found in [9]. The equivalent energy concept mentioned above is to give readers some basic idea of equivalent energy.

2.2 Application of Linear Cumulative Damage Rule and Rainflow-counting Algorithm

2.2.1 Linear cumulative damage rule

The linear cumulative damage rule, also called Miner's rule, is a common method used for fatigue prediction for the last five decades. This method assumes that failure of a material will occur when damage approaches to 1. The total damage is a summation of damage for each cycle loading across all cycles. The equation can be expressed as

$$D = \sum_{i=1}^{k} \frac{n_i}{N_i} \quad (2.3)$$

where D is the damage term, n is number of cycles of stress level accumulated, and N is the total number of the fatigue life of the material, or the number of cycles occurring until material failure. According to Miner's rule, failure occurs when the value of D equals to one. This method calculates fatigue in the life cycle loading condition. However, Miner's rule cannot directly apply to the random loading case since the cyclic loading in every cycle could be different. To overcome the random loading condition, additional processing is necessary and will be introduced in the next section.

2.2.2 Rainflow-counting algorithm

The rainflow-counting algorithm is used mainly to reduce a varying loading to a simple loading spectrum. The detailed derivation of the rainflow-counting algorithm can be found in the open literature [28,29]. The method can be applied to calculate a variety of loading cases. Since the rainflow-counting algorithm converts the loading spectrum and makes it into a single loading value, Miner's rule can directly implement the value to calculate the accumulated damage. Finally, the fatigue life can be predicted by combining the two methods. Thus, the two methods play critical roles in the present approach.

2.3 Model Energy Using Linear Cumulative Damage Rule

The definition of energy under the current model is the same as the energy model proposed by Wei [9]. However, the energy-based approach in Wei's study is only used to calculate the constant loading case. To handle random loading cases, more processes need to be involved. The present study proposes and verifies an alternative method to solve the random loading case. Specifically, I propose combining the rainflow-counting algorithm and damage cumulative rule to process random loading. The method involves the following steps.

First, the equivalent energy is calculated by the stress and strain data so that the stress and strain history would be input. Next, the input data would be used to calculate energy. The dilatational energy and distortional energy can be calculated separately and the equivalent energy can be calculated using Eq. 2.4. The rainflow-counting algorithm is then applied to gather each dilatational energy spectrum and distortional energy spectrum. Afterward, Miner's rule is implemented. The damage accumulated function, both for dilatational energy and distortional energy, can be expressed as

$$\begin{cases} D_{U_{dil}} = \sum_{i=1}^{N_{U_{dil}}} \frac{1}{f(U_{dil}^{i})} \\ D_{U_{dis}} = \sum_{i=1}^{N_{U_{dis}}} \frac{1}{f(U_{dis}^{i})} \end{cases} \tag{2.4}$$

where D represents the damage; $N_{U_{dil}}$ and $N_{U_{dis}}$ are number of cycles of dilatational energy and distortional energy spectrum, respectively, after applying the rainflow-counting algorithm; and $f(U^i)$ is the fatigue function of the energy with i representing the number of cycles. The two equations represent summation of the damage of energy random spectrum. Next, rewriting the equation for the total damage by using two energy terms, the equations can be expressed as

$$\begin{cases} D_{U_{dil}} = N^{eq} \times \frac{1}{f(U_{dil}^{eq})} \\ D_{U_{dis}} = N^{eq} \times \frac{1}{f(U_{dis}^{eq})} \end{cases} \tag{2.5}$$

where N^{eq} is the number of cycles for dilatational energy and distortional energy, and N^{eq} is also used to represent the total number of cycles from the rainflow-counting algorithm. Each energy is associated with a damage value which is calculated from the two energy spectrums and can be acquired using the following equations.

$$\begin{cases} U_{dil}^{eq} = f^{-1}(\frac{N^{eq}}{D_{U_{dil}}}) \\ U_{dis}^{eq} = f^{-1}(\frac{N^{eq}}{D_{U_{dis}}}) \end{cases} \tag{2.6}$$

The equivalent dilatational energy and distortional energy are obtained from Eq.2.6. The equivalent dilatational energy and distortional energy can then be converted to the total energy using the equivalent energy concept proposed by Wei [9]. Eq.2.1 shows the relationship between the total energy and the two separate energies. Finally, the fatigue life can be directly calculated by the equivalent energy fatigue prediction model. The equation of the fatigue life prediction model can be modified and expressed as

$$U_{N_f}^{eq} = f(N_f) \tag{2.7}$$

where $U_{N_f}^{eq}$ is the equivalent energy converted from dilatational energy and distortional energy and corresponds to the uniaxial equivalent Energy-N curve. The energy which is caused by torsion loading data has been transferred to the uniaxial energy data while the

hydrostatic energy is also transferred to uniaxial energy data. The detail for the equation derivation can be found in the energy-based model [9].

2.4 Validation

The proposed model is valid for Aluminum T7075-T651 experimental data that include different loading paths and loading types including uniaxial and multiaxial loading. The data on the material were collected by random loading cases which include several spectrums. Both predicted results of uniaxial and multiaxial loading spectrums are shown in Fig. 1. More data and details will be discussed in the next chapter.

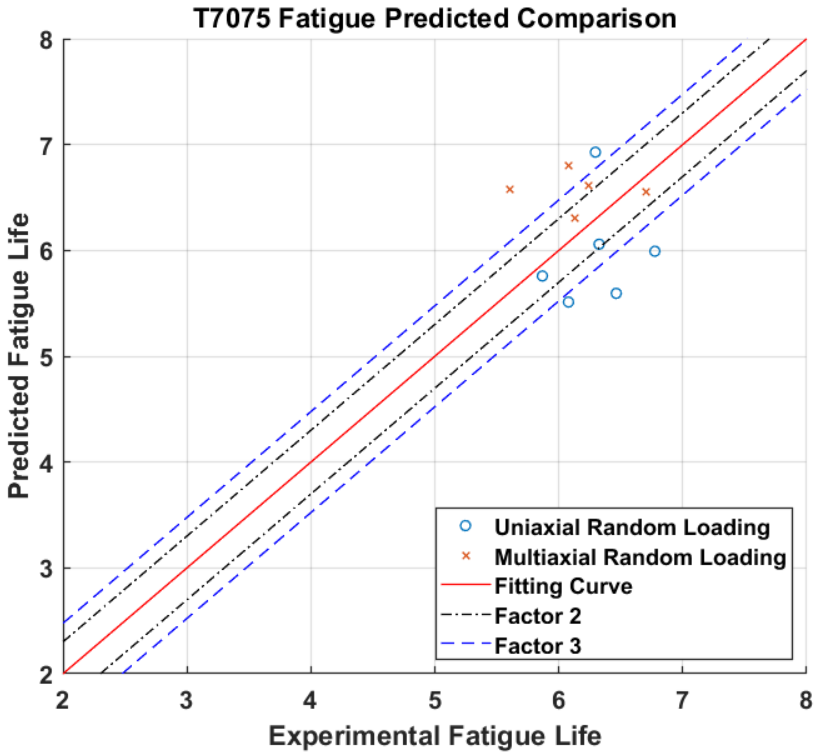

Fig. 1 Comparison Between Predicted and Experimental Fatigue Life Under Al T7075

2.5 Conclusion

A modified energy-based model is proposed. The proposed model can calculate fatigue life under random loading cases by combining rainflow-counting algorithm and

Miner's rule. The rainflow-counting algorithm reduces the complex loading cases to an equivalent constant loading case. The fatigue life can be calculated by Miner's rule that obtains corresponding damage in the different loading cycles. Two different loading path datasets under random loading case have been tested by the proposed model. The result shows that the accuracy of most data points is outside of error factor 3. Even though the modified energy-based model can handle random loading cases, the predicted accuracy needs to be improved. Therefore, the second energy-based model is proposed.

CHAPTER 3

3 TIME-BASED FATIGUE LIFE PREDICTION MODEL USING ENERGY-BASED METHOD

In this study, the equivalent energy also needs to be implemented in the first step. The details of the equivalent energy concept have been discussed in section 2.1. The time-based model of process is illustrated in Fig. 2. The detailed derivations will be discussed in the following section.

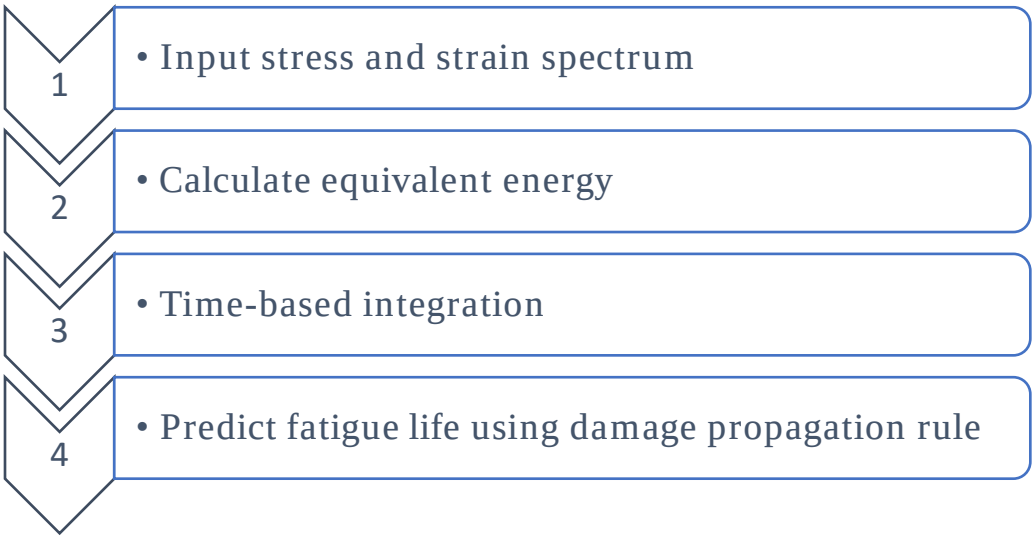

Fig. 2 Time-based Fatigue Model Flow-Chart

The time-based integration concept can be easily illustrated; Fig. 3 shows the relationship between the equivalent energy and time. The shaded area corresponds to the damage. The damage value at every time point can be calculated directly by integrating time. For instance, the damage value in the current cycle can be calculated by taking integration from the minimum energy to the maximum energy. In addition, the damage value can be an accumulation from the minimum energy to the maximum energy. The time range can be divided into four areas by selecting five points in the range between the minimum energy and the maximum energy. The damage value can be determined directly by this process. Therefore, the fatigue life can be easily predicted by this concept.

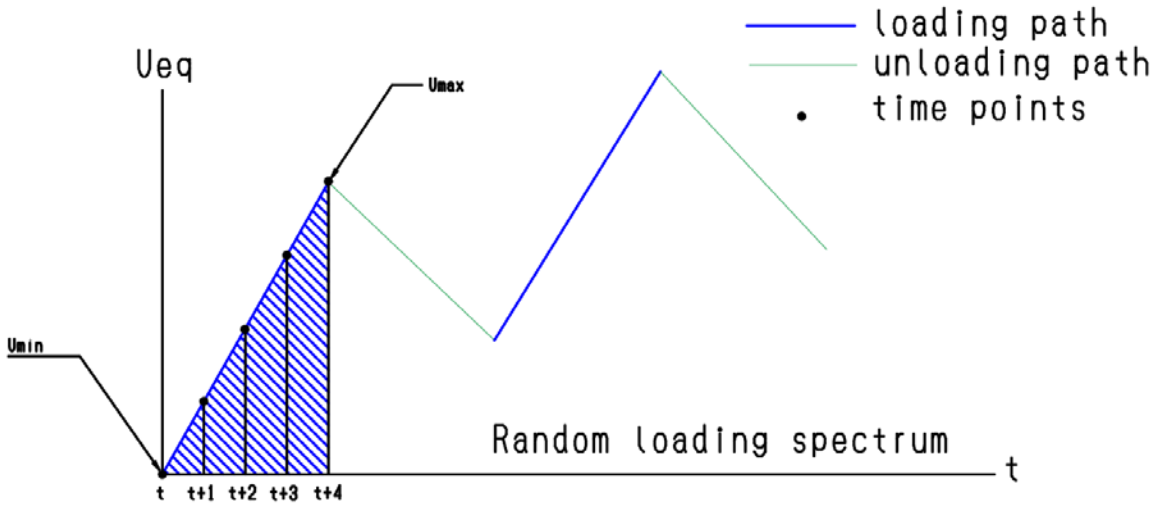

Fig. 3 Time-Based Integration Concept

3.1 Damage Propagation Based on Paris' Law Development

Cracks are commonly observed in mechanical components. After applying cycle loading for a period of time, a crack would initially grow very slowly but grow more quickly toward the end. This phenomenon is called fatigue crack propagation. Before explaining fatigue crack propagation, an important concept in fracture mechanics, stress intensity factor (SIF), will be introduced. The SIF describes the relationship between the crack propagation rate and the stress state at a crack tip. The function of SIF is shown as

$$K = Y\sigma\sqrt{\pi a} \qquad (3.1)$$

where K is the stress intensity factor, Y is the geometric value, σ is stress, and a is the crack length. Since the cyclic loading would be applied to the material, the applied stress would be defined as a range. The change of the function can be defined as

$$\Delta K = Y\Delta\sigma\sqrt{\pi a} \qquad (3.2)$$

where $\Delta\sigma$ is the stress range from minimum to maximum stresses (also can be expressed as $\Delta\sigma = \sigma_{max} - \sigma_{min}$). The relationship between fatigue crack propagation and SIF will be discussed in the next paragraph.

The formula for rate of crack growth in the number of cycles is represented as $\frac{\Delta a}{\Delta N}$. The crack propagation rate is driven by the stress intensity range ΔK and the expression can be shown as a differential form, $\frac{da}{dN}$. The crack propagation rate is shown as a curve in Fig. 4.

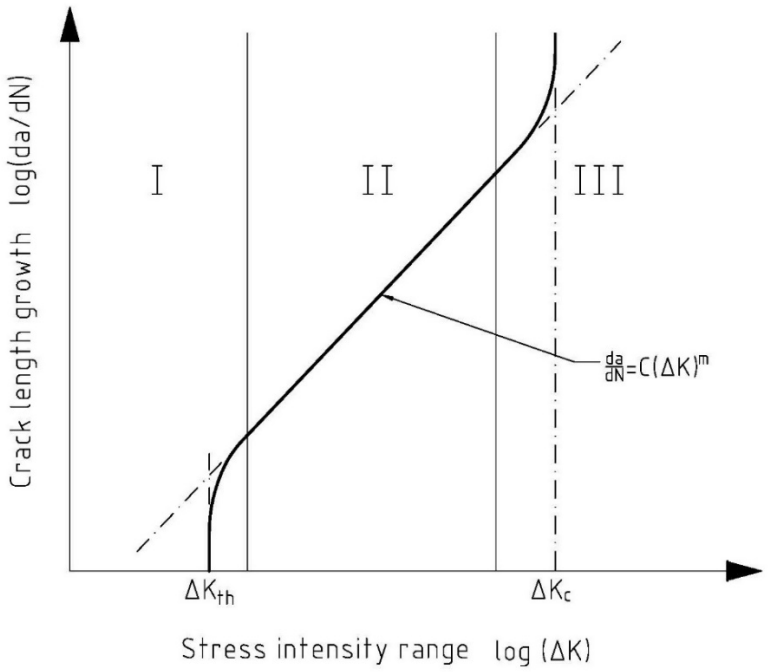

Fig. 4 The Relationship Between Crack Length Growth Rate and Stress Intensity Range in Log Scale

In the traditional theory there are three phases in the fatigue crack propagation. Phase I is the value below the K_{th} point. The crack propagation is difficult to observe; it hardly grows in this region. Thus, the crack would not propagate in the material below the threshold value. When the crack grows continuously beyond the K_{th} point and grows into the next region, the curve will become a straight line -- that is phase II. Phase II is the most important region and is the focus of this study. In Phase II, there is a linear relationship between $\log \frac{da}{dN}$ and $\log(\Delta K)$. After the linear relationship, the crack keeps growing into the next phase – Phase III. When the K value approaches this region, the stress intensity will

increase dramatically and the material will fail when the value approaches the critical point, K_c. The K value depends on crack length. The relationship of SIF and stress range can be found in Eq. 3.2.

Phase II will be discussed in more detail in the following. The linear relationship of crack length and SIF is known as Paris' curve or Paris' law. The equation of this straight line can be expressed as

$$\frac{da}{dN} = C(\Delta K)^m \tag{3.3}$$

where C and m are material fitting parameters. Integrating Paris' law allows us to calculate the fatigue life directly when phase II includes the significant part of the fatigue life. In this study, a new damage fatigue concept is implemented. Paris' law enables us to calculate fatigue life by calculating the crack length; by the same token, calculating damage enables us to acquire the corresponding fatigue life. Therefore, damage D is introduced here and it replaces the original crack length to represent a new function. The function can be shown as

$$\frac{dD}{dN} = C(\Delta K)^m \tag{3.4}$$

where $\frac{dD}{dN}$ is the damage per cycle, and the rest of the parameters are the same as Eq. 3.3. The original definition for ΔK is equal to $(K_{max} - K_{min})$; this ΔK is the original stress intensity factor. Now the damage concept that is mentioned above is implemented by replacing the crack length by the damage parameter. Therefore, the SIF equation can be rewritten as

$$\Delta K = \Delta\sigma\sqrt{\pi D} \tag{3.5}$$

It is assumed that the geometric function can be ignored so that Y is equal to 1 since the predicted process does not consider the geometric shape.

With the damage propagation being defined above, the term energy will be defined as the following. Since the stress-based approach applies to high cycle fatigue, the energy phase in this study is expected to be applicable in various conditions no matter HCF or LCF. The energy range is defined as

$$\Delta U = (U_{max} - U_{min}) \qquad (3.6)$$

where ΔU is the energy range, U_{max} is maximum energy, and U_{min} is minimum energy.

Note that the two terms, stress and energy, are based on different concepts. The energy term cannot be less than zero. Thus, replacing stress with energy in the following equation is the first step. The relationship between stress and energy is shown as

$$\sigma = \sqrt{2EU} \qquad (3.7)$$

where E is Young's modulus, energy is U, and σ is stress. Since the basic knowledge is based on the strain density energy formula, the stress is directly relative to energy. Now, the domain of the method is changed from stress-based to energy-based. As mentioned before, the energy-based method enables us to deal with both high cycle fatigue and low cycle fatigue which both apply to elastic region and plastic region fatigue life prediction. Note that the stress spectrum with no mean stress can be shown as Fig. 5. The energy spectrum after transferring from stress spectrum can be shown as Fig. 6. Thus, the SIF is related to energy.

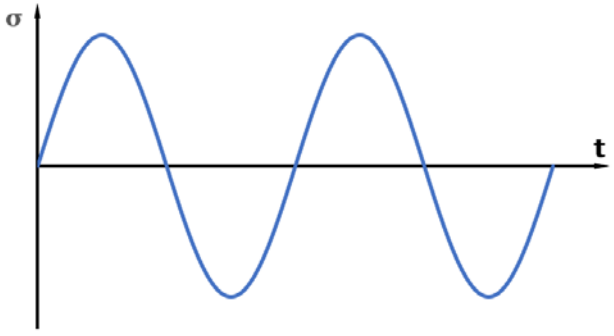

Fig. 5 Stress Spectrum

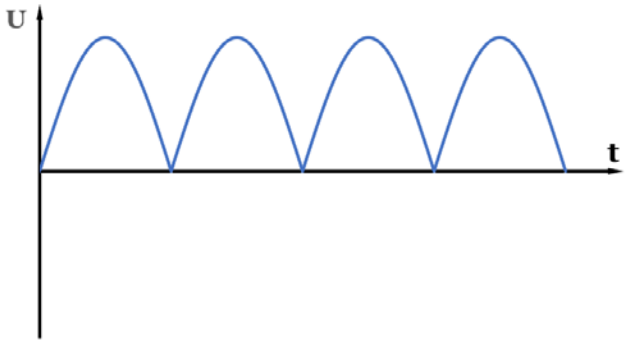

Fig. 6 Energy Spectrum

The K_{min} can be determined to be zero since the minimum energy is zero when the stress has no mean value. The equation can be converted as

$$\frac{dD}{dN} = C\,(K-0)^m = C\,(\sqrt{2\pi DEU})^m \qquad (3.8)$$

The cycle-based method in energy phase which is computed based on the modified Paris' law is also called damage propagation function in energy phase. Thus, the fatigue life can be calculated from Eq. 3.8 under the cycle-based method. The following steps show the derivative equations. After rearranging Eq. 3.8, the equation can be expressed as

$$D^{-\frac{m}{2}}dD = C\,(2\pi E)^{\frac{m}{2}}U^{\frac{m}{2}}dN \qquad (3.9)$$

To calculate the relationship between damage and energy, taking the integration for Eq. 3.9 is essential. The integrating range for damage is from initial damage to one which means the whole damage process in the material. When the damage value approach 1, it is assumed that the material will fail at that point. On the other hand, the fatigue life is from 0 to N_f. The variable N_f is the predicted fatigue life. The equation can be expressed as

$$\int_{D_0}^{1} D^{-\frac{m}{2}}dD = \int_{0}^{N_f} C\,(2\pi E)^{\frac{m}{2}}U^{\frac{m}{2}}dN \qquad (3.10)$$

Therefore, the power function can obtain the fatigue life by solving Eq. 3.10.

$$N_f = \frac{2}{C(2-m)}\left(1 - D_0^{\frac{2-m}{2}}\right)(2\pi E)^{-\frac{m}{2}}U^{-\frac{m}{2}} \qquad (3.11)$$

Eq. 3.11 represents a power function Therefore, the energy-curve power function, which is calculated from experimental tension and torsion datasets, can assist to find C and m values. The energy-curve power function can be expressed as

$$U = p \times {N_f}^q \tag{3.12}$$

U is energy, N_f is fatigue life from the experimental data, and p, q are constant. Hence, the C and m can correspond to p and q by solving Eq. 3.11 and Eq. 3.12. The parameter relationship is shown as

$$\begin{cases} C = \frac{2}{(2-m)}(1 - D_0^{\frac{2-m}{2}})(2\pi Ep)^{-\frac{m}{2}} \\ m = -\frac{1}{q} \end{cases} \tag{3.13}$$

Although this function can calculate fatigue life, there is a drawback. When the cycle-based approach is applied to a random loading condition, it cannot calculate predicted life directly since the stress or energy range are different in every cycle. Thus, one additional process must be considered. The rainflow-counting algorithm will be applied to deal with various loading cases. One of the study ideas is inspired by removing this step. For the damage propagation equation along with the energy-based model, the constant loading cases in both high cycle fatigue and low cycle fatigue can be solved. However, the random loading cases cannot be solved with the cycle-based model. To overcome this problem that avoids using the rainflow-counting algorithm, the new concept must be involved. Thus, the sub-cycle which is also called time-based method is used to deal with the random loading cases. The detail will be found in section 3.3.

3.2 Sub-cycle Damage Growth Function Development

The sub-cycle concept, also called the time-based concept, is used to calculate the cyclic loading spectrum in every moment of time. The sub-cycle fatigue crack growth function, which is proposed by [27], is based on this concept. The approach is applied to

deal with various loading cases. Also, the crack length can be calculated by integrating the loading spectrum. Integrating the sub-cycle crack growth function for one cycle can obtain the relationship between crack growth rate per cycle and energy function [27]. The expression is shown as

$$\frac{da}{dN} = \int_{\sigma_{op}}^{\sigma_{max}} \frac{da}{d\sigma}(\sigma, \dot{\sigma}, a, E, \sigma_y \dots) d\sigma \qquad (3.14)$$

where $\frac{da}{dN}$ is crack length per cycle, σ_{max} and σ_{op} are maximum and opening stress, respectively. $\frac{da}{d\sigma}(\sigma, \dot{\sigma}, a, E, \sigma_y \dots)$ is a sub-cycle crack growth function that depends on stress σ, loading rate $\dot{\sigma}$, crack length a, Young's modulus of material E, yield stress σ_y, and other parameters that contribute to this equation. In this function, the crack growth only considers from σ_{op} to σ_{max} and there is no crack growth in the unloading area. Other than the sub-cycle crack growth function, there is another important concept needed to be discussed. The detail will be shown below.

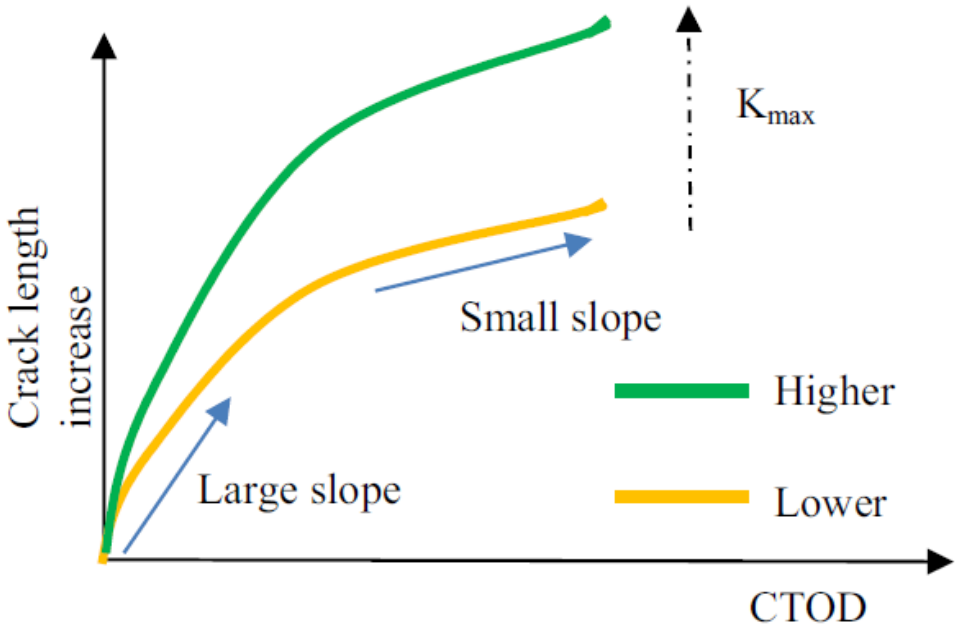

Fig. 7 The Relationship of Crack Length Increase Rate and CTOD at Sub-Cycle Scale [27]

The proposed approach is a sub-cycle crack growth function through a geometrical relationship between incremental crack growth da and the change in the crack tip opening displacement (CTOD)[30]. The CTOD is a critical concept in the sub-cycle crack growth function. The CTOD increases when the crack starts to open. However, the detail about CTOD is not discussed here. More information can be found in situ SEM testing research [31,32]. Only a few important concepts will be mentioned in this study. Fig. 7 shows a nonlinear relationship between crack length and CTOD. The phase II segment in Fig. 4, the curve, can be observed through a power function. K_{max} is the maximum stress intensity factor. The power function also depends on K_{max}. The tendency observed is such that a larger slope in the curve means a smaller maximum stress intensity factor and vice versa. The curve, a power function, can be expressed as

$$\Delta a = AK_{max}^{B}\delta^{d} \tag{3.15}$$

where Δa is the incremental crack length in the current cycle, A and B are fitting parameters, δ is the CTOD which is considered as the crack growth during the increasing part of the loading portion, and d is the material parameter.

After introducing the two kernel sections of the sub-cycle crack growth function, the next step is to determine the sub-cycle damage growth function. The idea of the sub-cycle damage growth function is the same as in the previous section which replaces crack length with damage. The first is to determine the equation that can describe the relationship between damage and CTOD. Thus, the Eq. 3.15 can be rewritten as

$$\Delta D = AK_{max}^{B}\delta^{d} \tag{3.16}$$

where ΔD is incremental damage in the current cycle, and the other parameters are the same as those in Eq. 3.15. Taking the differential form for both sides of Eq. 3.16, the equation can be expressed as

$$\frac{dD}{dt} = AK_{max}^{B}\delta^{d-1}\frac{d\delta}{dt} \tag{3.17}$$

where $\frac{dD}{dt}$ is the damage growth rate, and $\frac{d\delta}{dt}$ is the CTOD change rate. The K_{max} can be written as

$$K_{max} = \sigma_{max}(\pi D)^{\frac{1}{2}} \tag{3.18}$$

where K_{max} is the largest intensity factor, σ_{max} is the maximum stress, and D is the damage in the current state. Note that K_{max} is the largest stress intensity factor from the previous loading. When the K_{max} is in a constant loading case, the value can be considered as a constant. On the other hand, a random loading case includes different K_{max} values in the various waveform. Before entering the next step, the CTOD will be mentioned here. The relationship between stress intensity factor and CTOD is shown as

$$\delta = \frac{\Delta K_{eff}{}^2}{2E\sigma_y} = \frac{(0.6\Delta K)^2}{2E\sigma_y} \tag{3.19}$$

where ΔK is the stress intensity factor range, E is Young's modulus, and σ_y is yield strength. The minimum energy value is zero when the stress spectrum has no mean stress, which is mentioned above. The equation can be expressed as

$$\delta = \frac{(0.6K-0)^2}{2E\sigma_y} = \frac{(0.6K)^2}{2E\sigma_y} \tag{3.20}$$

The equation can be expressed as Eq. 3.21 after substituting the largest SIF and CTOD in the original damage growth function.

$$\Delta D = A[\sigma_{max}(\pi D)^{\frac{1}{2}}]^B \left(\frac{\sigma^2\pi D}{2E\sigma_y}\right)^d \tag{3.21}$$

Now, the damage growth function is shown as a stress-based function. To apply more situations such as the energy-based model mentioned earlier, this equation needs to be converted from a stress-based to energy-based function. Eq. 3.7 is applied to replace the stress with energy and the maximum stress intensity factor also will be converted to the maximum energy intensity factor. The equation can be expressed as

$$K_{max} = (2\pi DEU_{max})^{\frac{1}{2}} \tag{3.22}$$

where K_{max} is the maximum energy intensity factor, D is damage, E is Young's modulus, and U_{max} is maximum energy. Now, all stress terms are transferred to energy phase terms which means that the function can be applied in both HCF and LCD while managing the constant loading and various loading in the time-based damage propagation function. When Eq. 3.7 and Eq. 3.22 are substituted in Eq. 3.16, the equation will be shown as

$$\Delta D = A(2\pi DEU_{max})^{\frac{B}{2}}(\frac{2\pi DEU}{2E\sigma_y})^d \qquad (3.23)$$

where ΔD is incremental damage. Eq. 3.23 can be taken as a derivative to represent a continuous form as

$$\frac{dD}{dU} = Ad(2\pi EU_{max})^{\frac{B}{2}}(\frac{\pi}{\sigma_y})^d D^{\frac{B}{2}+d}U^{d-1} \qquad (3.24)$$

Eq. 3.24 is derivative by time. Thus, using the same technique as Eq. 3.14, the function integrates a complete cycle to acquire the damage increment per cycle. The time-based concept can be involved to calculate the value while modifying Eq. 3.14 to a damage-energy form. The equation can be expressed as

$$\frac{dD}{dN} = \int_{U_{min}}^{U_{max}} \frac{dD}{dU}\left(U, \dot{U}, D, E, \sigma_y \dots\right)dU \qquad (3.25)$$

where $\frac{dD}{dN}$ is damage per cycle, U_{max} and U_{min} is maximum energy and minimum energy, respectively. Note that the minimum energy is used here since the energy intensity factor range is converted to minimum loading level but not opening loading level and the minimum is assumed to be zero. The $\frac{dD}{dU}\left(U, \dot{U}, D, E, \sigma_y \dots\right)$ is a sub-cycle damage growth function that depends on energy U, energy rate $\dot{U}$, damage D, Young's modulus of material E, yield strength σ_y, and any other parameter that can contribute to this equation. The equation after applying Eq. 3.25 can be expressed as

$$\frac{dD}{dN} = 2Ad(2\pi EU_{max}^{his})^{\frac{B}{2}}(\frac{\pi}{\sigma_y})^d D^{\frac{B}{2}+d}\int_{U_{min}}^{U_{max}} U^{d-1}\,dU \qquad (3.26)$$

where $\frac{dD}{dN}$ is damage increment per cycle, $\int_{U_{min}}^{U_{max}} U^{d-1}\, dU$ is the accumulated energy in the current completed cycle. U_{max}^{his} depends on the loading cases. If there is constant loading, the value is the same as the maximum energy U_{max} in the equation. If there is various loading, the value would be a memory maximum energy which is collected by presenting one hundred cycles maximum energy and selecting the largest one of the values from the cycles. Other parameters are the same as mentioned before. The main purpose in this function is to first, gather the damage at every time point loading history. Then, take the integration for a complete cycle to obtain the corresponded damage per cycle. The significant advantage is that even though there is different damage in various loading conditions, every cycle collect its damage. Hence, the fatigue life can be precisely calculated by integration. The material will fail when the value of damage grows and the value approaches 1. In other words, the damage can continuously accumulate to a certain value to correspond to the fatigue life. Now, the following steps are shown in the whole process. The complicated formula is simplified by an α to make the equation more understandable. The equation is expressed as

$$\alpha = A(2\pi E U_{max}^{his})^{\frac{B}{2}} (\frac{\pi}{\sigma_y})^{d} \qquad (3.27)$$

where α is expressed by this equation. Therefore, Eq. 3.26 can be rewritten as

$$\frac{dD}{dN} = 2d\alpha D^{\frac{B}{2}+d} \int_{U_{min}}^{U_{max}} U^{d-1}\, dU \qquad (3.28)$$

Eq. 3.28 represents a function of damage increment per cycle. After the equation is simplified by integrating the energy and rearranging it, the equation can be shown as

$$\frac{dD}{dN} = \alpha D^{-(\frac{B}{2}+d)}(U_{max}^{d} - U_{min}^{d}) \qquad (3.29)$$

Now, the equation is related to maximum energy and minimum energy. This damage function can directly calculate the fatigue life by using the peak and valley values from the loading spectrums. Since the time-based concept has been applied in this study, the

loading spectrums could include different frequency. Thus, the equation had to be changed phase from the cycle-based concept to the time-based concept. The equation can be expressed as

$$\frac{dD}{dN} = \alpha D^{-(\frac{B}{2}+d)}(U_{t+1}^{d} - U_{t}^{d}) \qquad (3.30)$$

where $\frac{dD}{dN}$ is damage increment per cycle, D is the current damage, U_{t+1} is the energy value at the next point, U_t is the energy value at the current point and d is the material parameter in damage propagation. In this study, the d is set as 0.01. Now, A and B are fitting parameters and still unknown. Therefore, the next step is using another technique to obtain the A and B parameters. In this section, the time-based damage propagation function was discussed.

Finally, the fatigue life can be calculated directly by accumulating every time step. The failure criterion is that the material fails when damage value approaches to 1. The equation can be expressed as

$$D_{N_f} = D_{t-1} + \frac{dD}{dN} \geq 1 \qquad (3.31)$$

3.3 Model Parameter Calibration

The unknown parameters still need to be determined by experimental data. For the previous section, the experimental data is verified for Eq. 3.17. Now, only the parameters in the time-based damage propagation function need to be clarified. The parameter calibration method will be used here [26]. The time-based function can be compared with Paris' law when the function is shown as Eq. 3.28. Since Eq. 3.28 is shown as damage per cycle $\frac{dD}{dN}$, the function can be corresponded as

$$\frac{dD}{dN} = C(\Delta K)^{m} = AK_{max}^{B}\delta^{d} \qquad (3.32)$$

Then, the CTOD can also be represented as Eq. 3.20 and these two equations are combined. The function will be express as

$$C(\Delta K)^m = AK_{max}^B(\frac{0.36\Delta K^2}{2E\sigma_y})^d \quad (3.33)$$

Therefore, comparing the parameters to fit the A and B. The material parameter d, depends on the material and will be added into the model. Since the open cracking needs to be considered, the parameter calibration can be classified as two parts separated by R ratio. When R ≥ 0, the fitting parameters can be shown as

$$\begin{cases} A = C(0.36)^{-d}(1-R)^B(2E\sigma_y)^d \\ B = m - 2d \end{cases} \quad (3.34)$$

Where C and m are fitted from the tension or torsion experimental data, R is the stress ratio which is calculated in loading spectrum, d is material parameter, E and σ_y are Young's modulus and yield strength, respectively, and A and B are the target fitting parameters.

When R < 0, the fitting parameters can be shown as

$$\begin{cases} A = C(0.36)^{-d}(1-R)^{B+2d}(1-\beta R)^{-2d}(2E\sigma_y)^d \\ B = m - 2d \end{cases} \quad (3.35)$$

β is calibrated with a negative stress ratio fatigue crack growth test. Detail about β can be found in [27]. It varies by different metal materials. The expression can be approximated as

$$\beta = 30.091\sigma_y^{-0.797} \quad (3.36)$$

Since the equivalent energy concept is used here, the mean stress is converted to zero so that Eq. 3.34 will only be used in the model. However, the spectrum that includes mean stress can still apply Eq. 3.35 to fit the parameters. Finally, the model parameter calibration confirmed the A and B as the last step. The model is ready to calculate the fatigue life now.

3.4 Model Validation

The proposed model is validated by several open literature [2,33–40]. The collected data include different loading paths and different materials. Fig. 8 shows the loading paths of the data used in the current study. The datasets include uniaxial and multiaxial loading. Most of the collected data apply to materials that have constant loading cases, and only one dataset applies to materials that have various loading. The data with various loading include several spectrums. The spectrums for HCF under multiaxial random loading cases are shown in Fig. 9. The spectrums for HCF under uniaxial random loading cases are shown in Fig. 10. The spectrums for LCF+HCF under uniaxial and multiaxial random loading cases are shown in Fig. 11. Table 1 summarizes the details of the fatigue testing spectrums under HCF and Table. 2 shows the spectrums under HCF+LCF. According to the hypothesis, this proposed model is suitable for both the tension-torsion state and the tension-tension state while it can also deal with different spectrums. In this report, the collected data are validated only by the tension-torsion state. Although this model can be applied to the biaxial loading cases, the validation by tension-tension loading cases can be studied in the future. Table. 3 shows the summary of the materials and several loading paths. The references are listed in the last column and the material properties can be found in the references. The results of the predicted fatigue life and experimental fatigue life in constant loading for seven materials are shown in Fig. 12. The fatigue life prediction of random loading for both uniaxial and multiaxial loading under Al T7075 is shown in Fig. 13.

Table 1. Summary of Fatigue Testing Spectrum Under Random Loading Conditions in HCF.

Spectrum name	Loading path	Fatigue life
Linear	Uniaxial	2,112,921
Simplified linear	Uniaxial	736,909
FELIX	Uniaxial	5,956,555
FELIX + 35	Uniaxial	1,971920
Modified FELIX	Uniaxial	2,905,820
Simplified max(FELIX) + 35	Uniaxial	1,196,807
Proportional FELIX	Multiaxial	1,338,786
Modified proportional FELIX	Multiaxial	1,745,638
CWT edited proportional FELIX	Multiaxial	5,106,200
Nonproportional FELIX	Multiaxial	1,191,522
Modified nonproportional FELIX	Multiaxial	405,053

Table 2. Summary of Fatigue Testing Spectrum Under Random Loading Conditions in HCF+LCF.

Spectrum name	Loading path	Fatigue life
Linear_HCF+LCF	Uniaxial	68,894
Nonlinear_HCF+LCF	Uniaxial	35,908
Proportional_HCF+LCF	Multiaxial	11,046
Nonproportional_HCF+LCF	Multiaxial	17,575

Table 3. Summary of Collected Experimental Data.

Material	Loading Path	Reference
AISI 304 Steel	Uni, Tor, Pro, Sin90	[33]
A533B	Uni, Tor, Pro, Sin90	[34]
S45C Steel	Uni, Tor, Pro, Sin90, Sin45, Sin22.5	[35]
SAE 1045	Uni, Tor, Pro, Sin90, box	[36]
S460N	Uni, Tor, Pro, Sin90	[37]
Al T6061	Uni, Tor, Sin90	[39]
Al T7075	Uni, Tor, Pro, Sin90	[2,40]

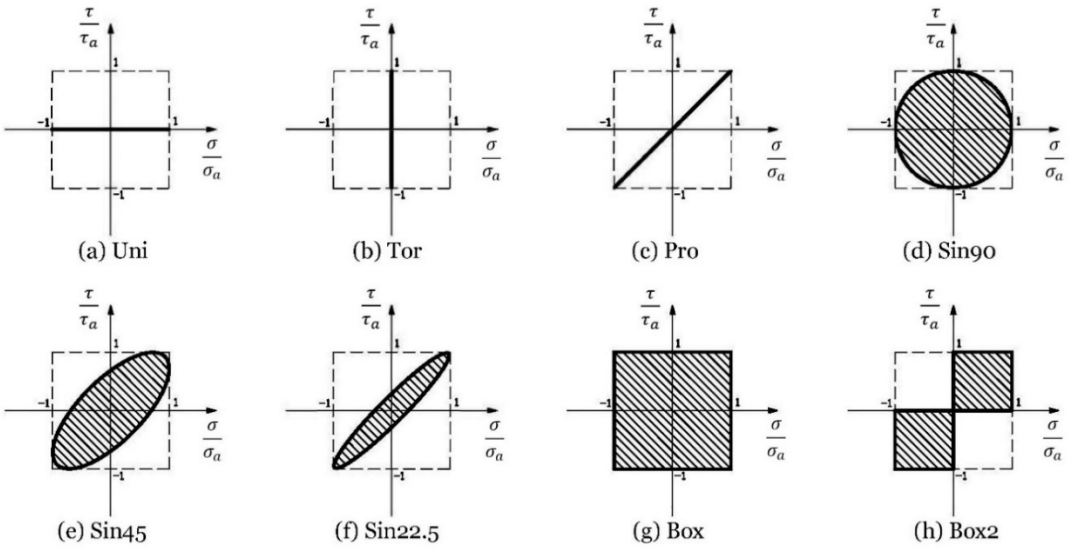

Fig. 8 Stress Paths of Data Used in the Current Study

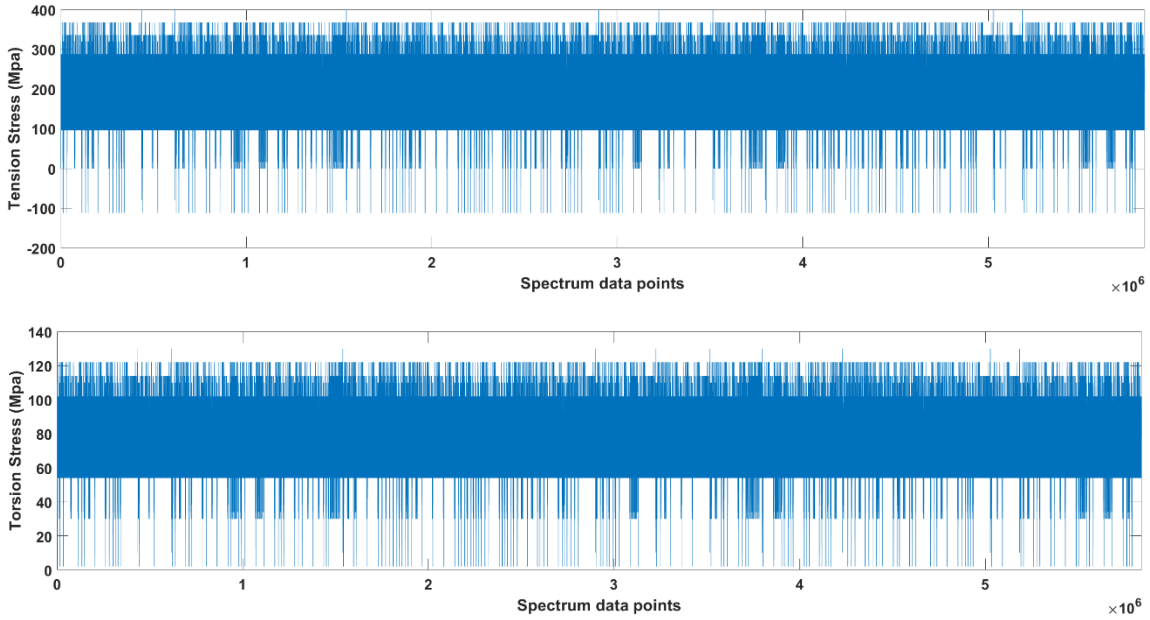

(a) Proportional FELIX Spectrum

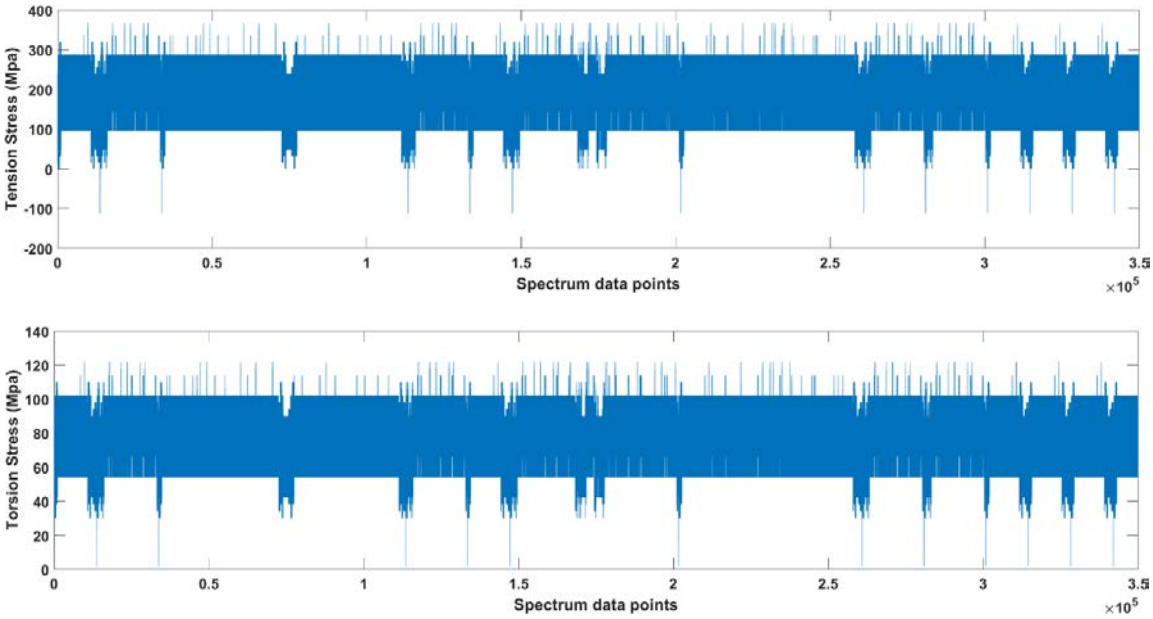

(b) Modified Proportional FELIX Spectrum

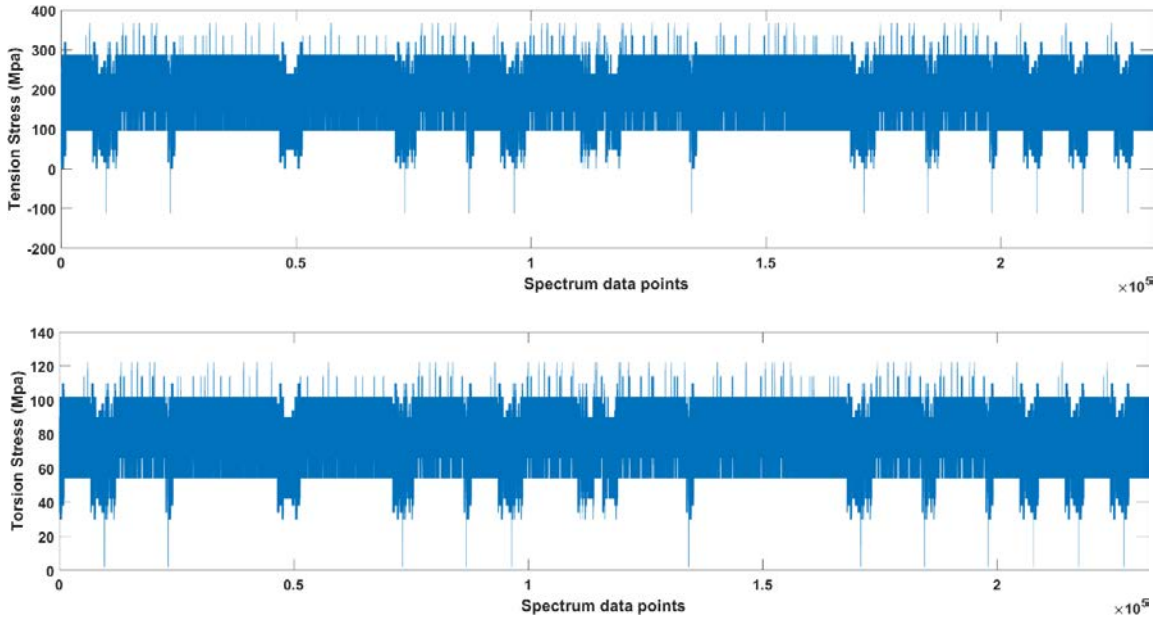

(c) CWT Edited Proportional FELIX Spectrum

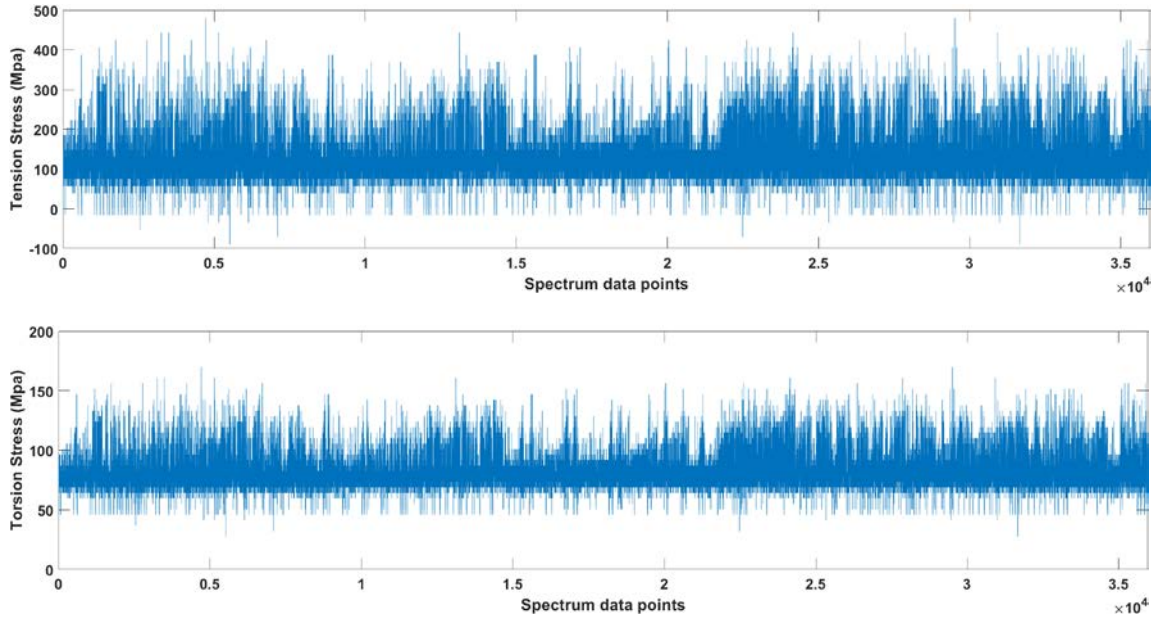

(d) Nonproportional FELIX Spectrum

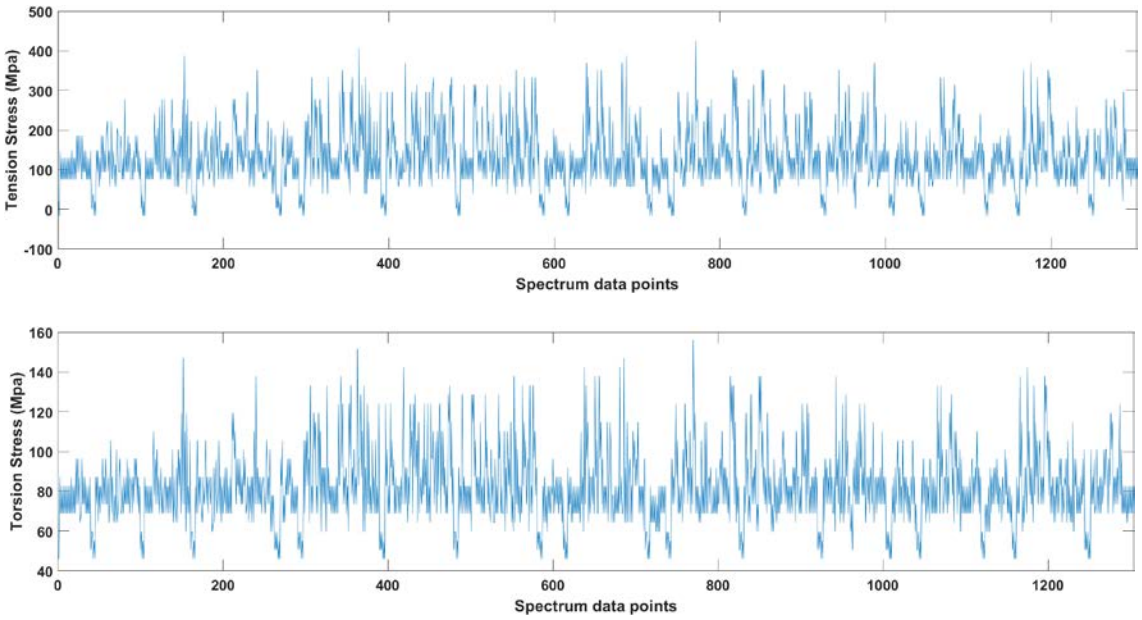

(e) Modified Nonproportional FELIX Spectrum

Fig. 9 Generated Spectrum for Fatigue Testing Under Multiaxial Random Loading

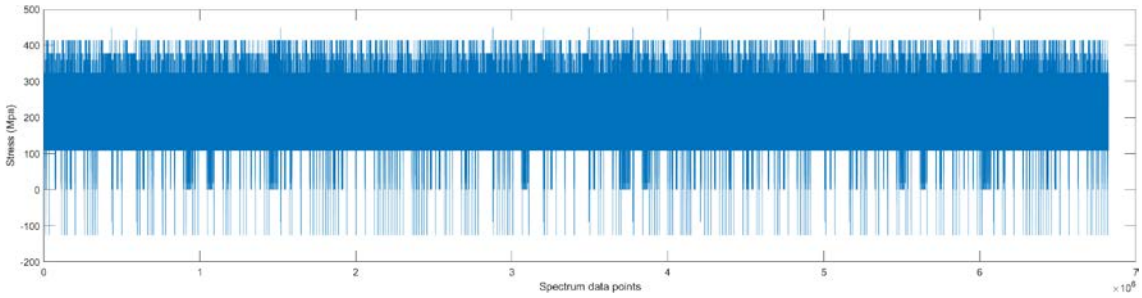

(a) FELIX Spectrum

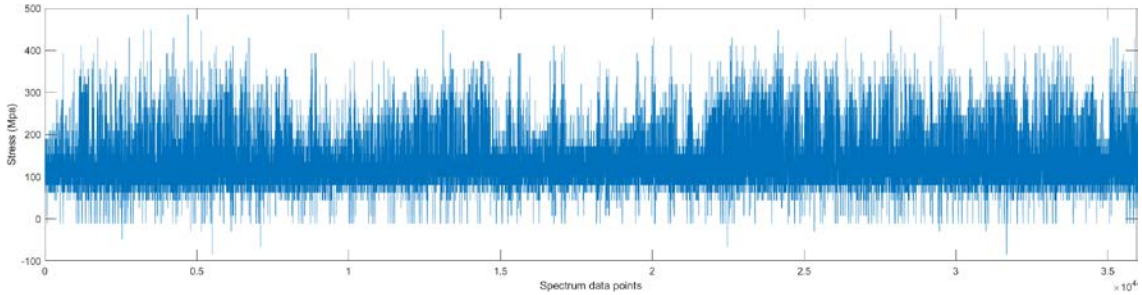

(b) FELIX + 35 Spectrum

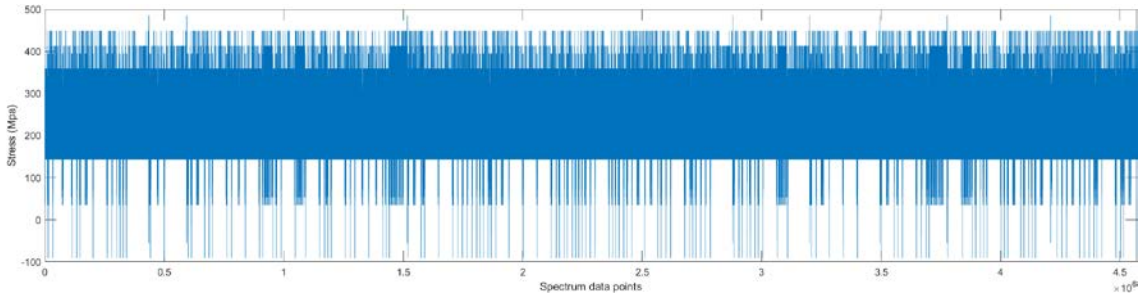

(c) Modified FELIX Spectrum

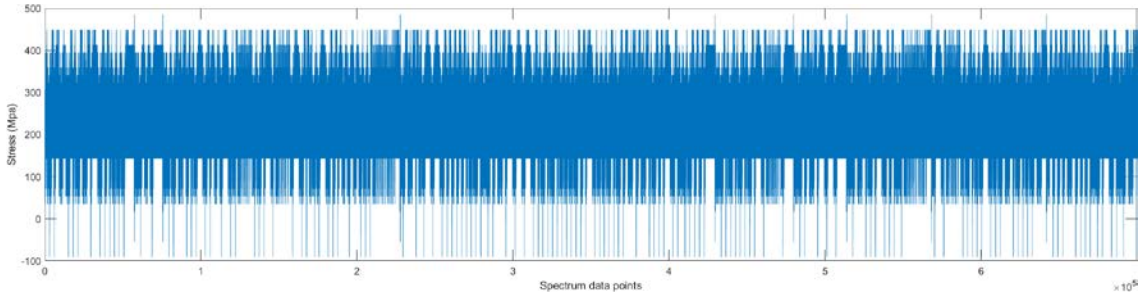

(d) Simplified Max(FELIX) + 35 Spectrum

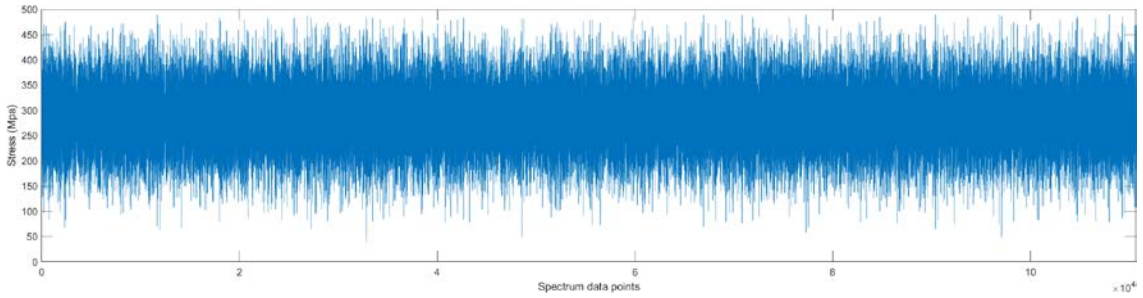

(e) Linear Spectrum

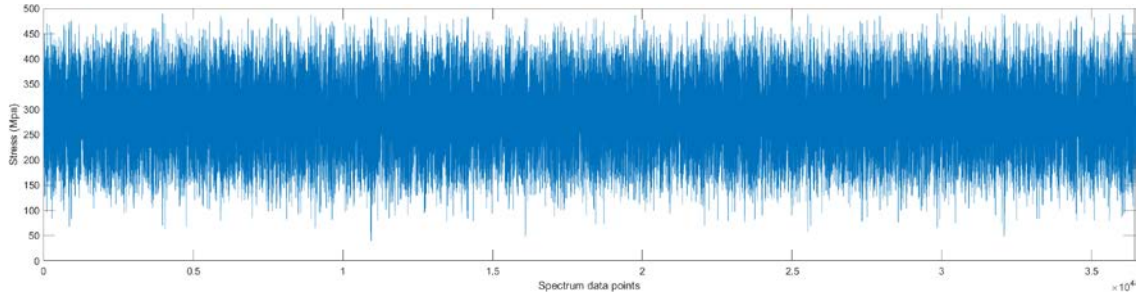

(f) Simplified Linear Spectrum

Fig. 10 Generated Spectrum for Fatigue Testing Under Uniaxial Random Loading

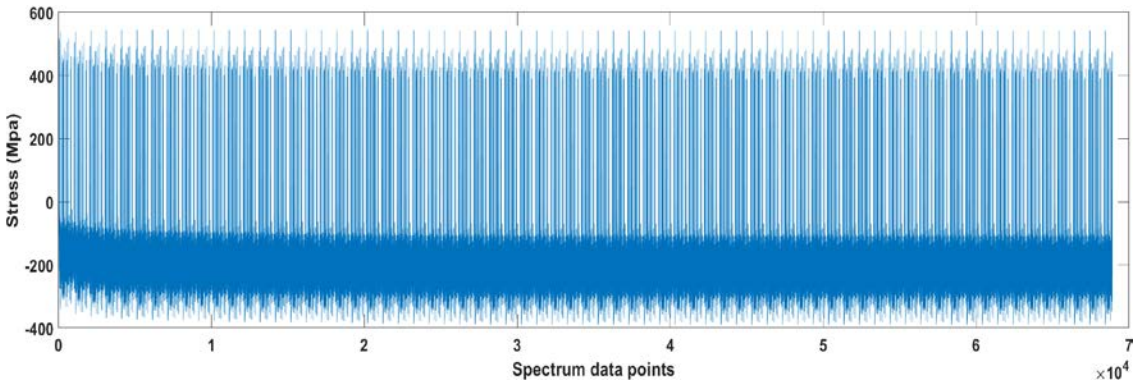

(a) HCF+LCF Linear Spectrum

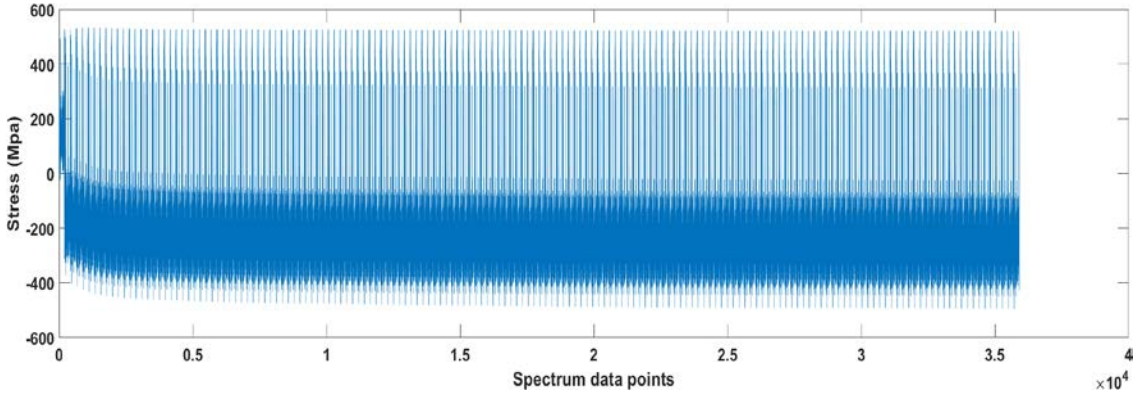

(b) HCF+LCF Nonlinear Spectrum

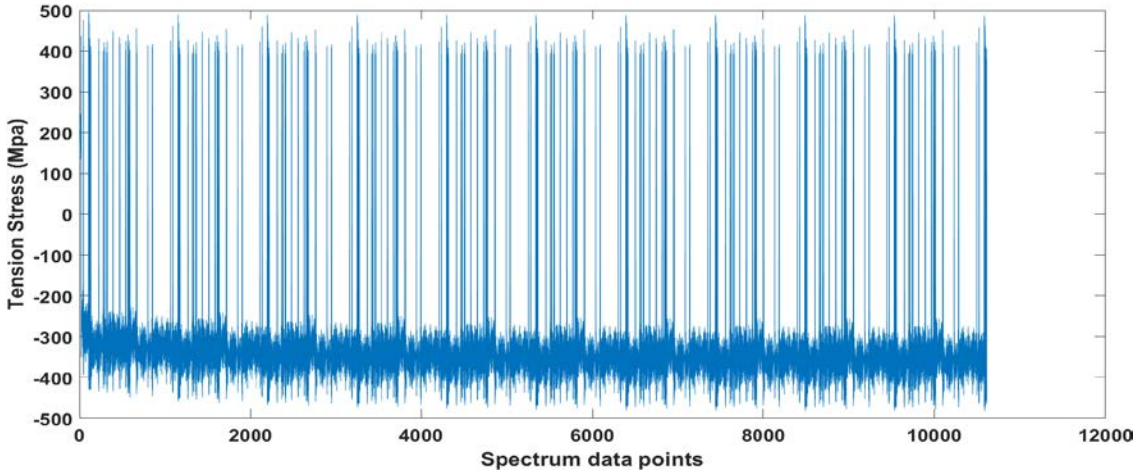

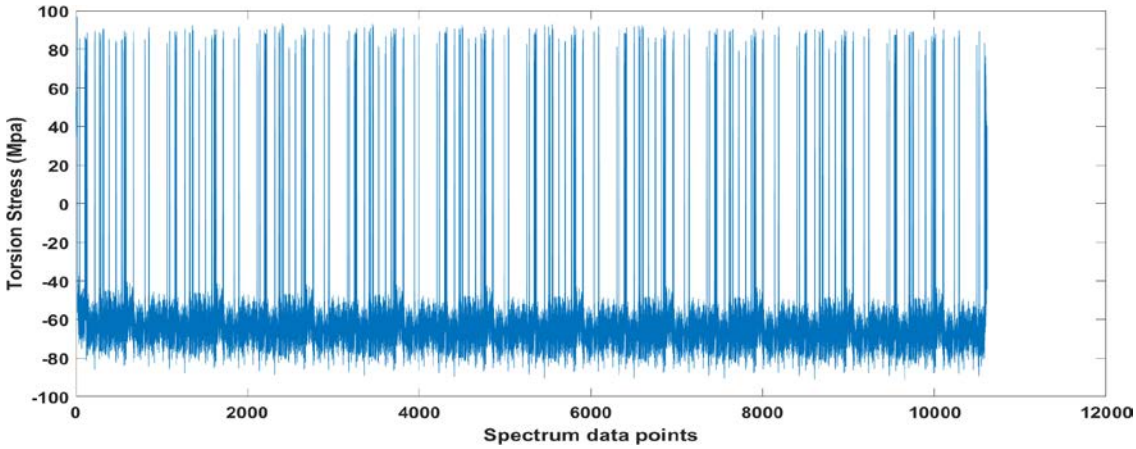

(c) HCF+LCF Proportional Spectrum

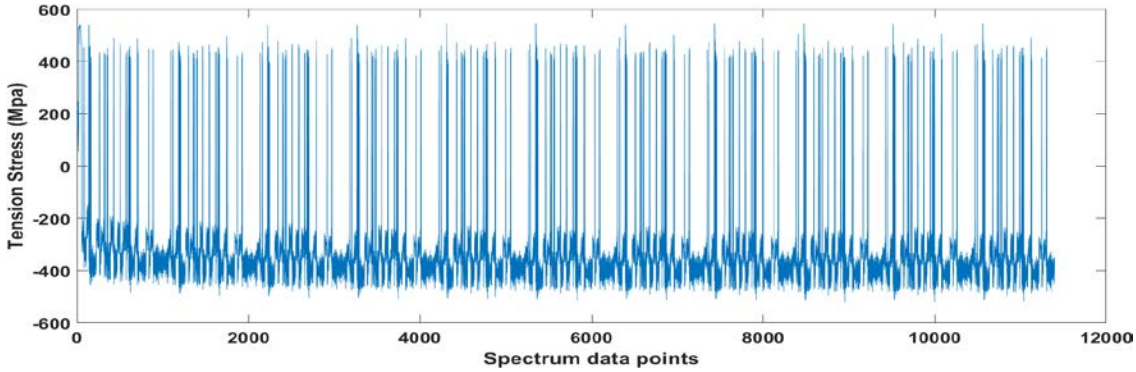

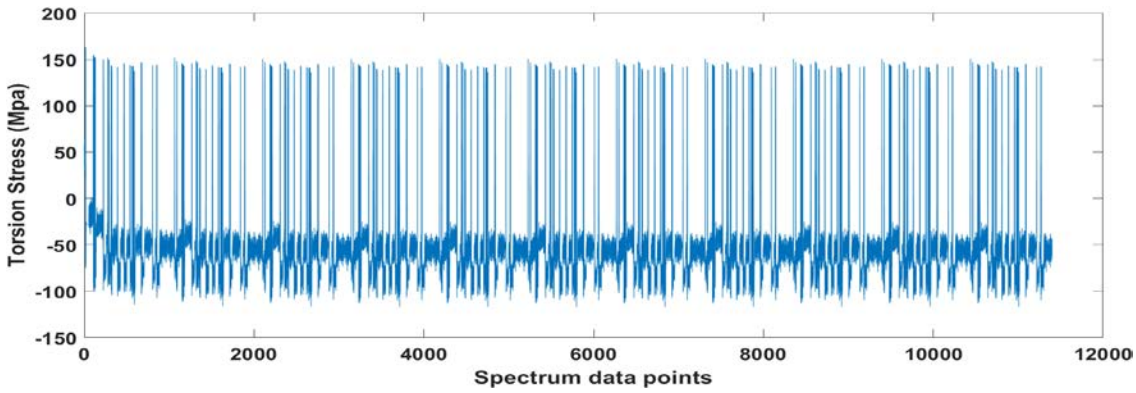

(d) HCF+LCF Proportional Spectrum

Fig. 11 HCF+LCF Spectrum for Fatigue Testing Under Multiaxial Random Loading

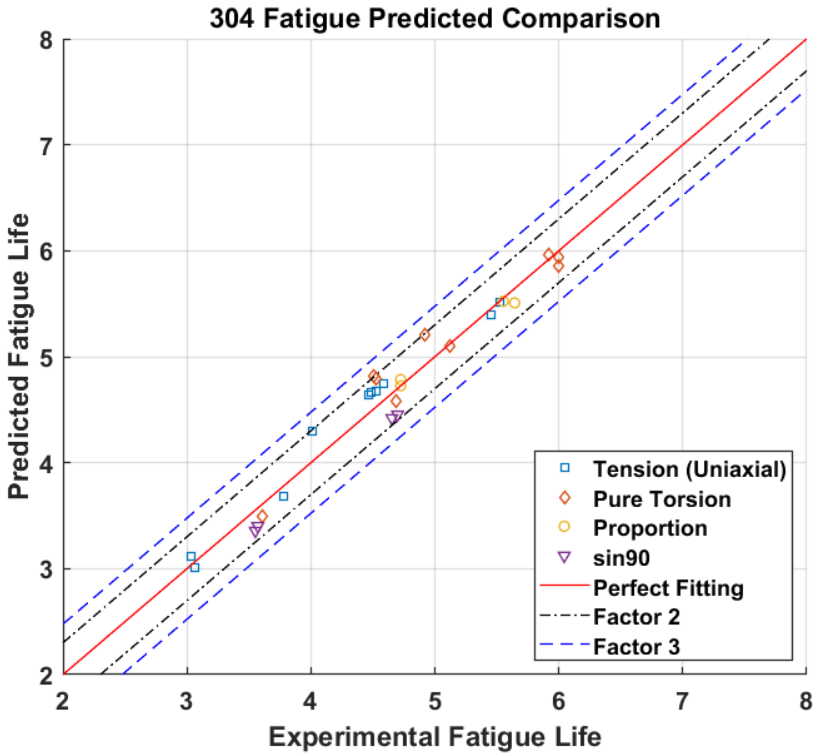

(a) AISI 304 Steel

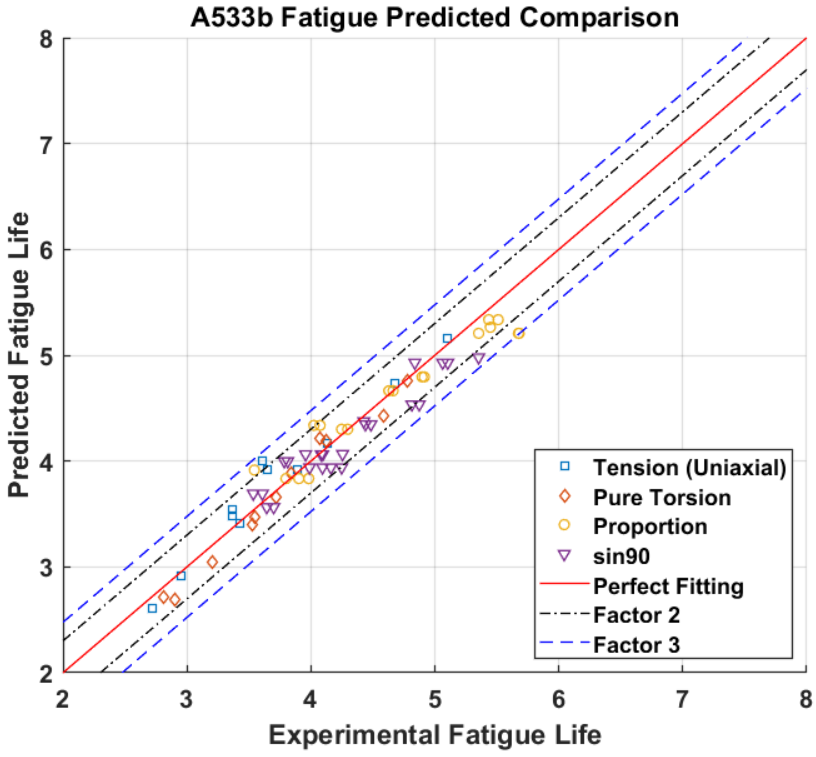

(b) A533B

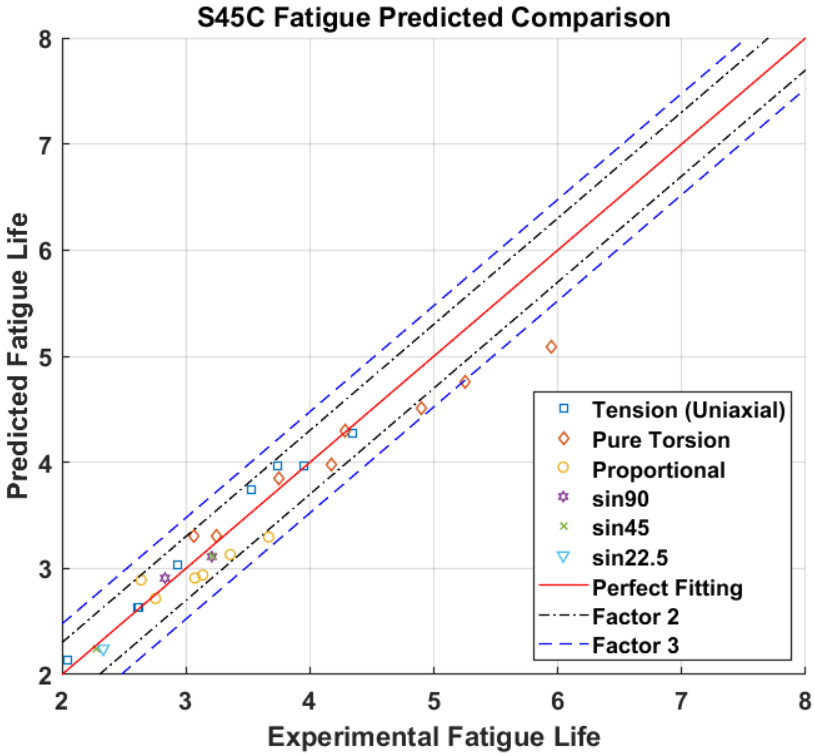

(c) S45C Steel

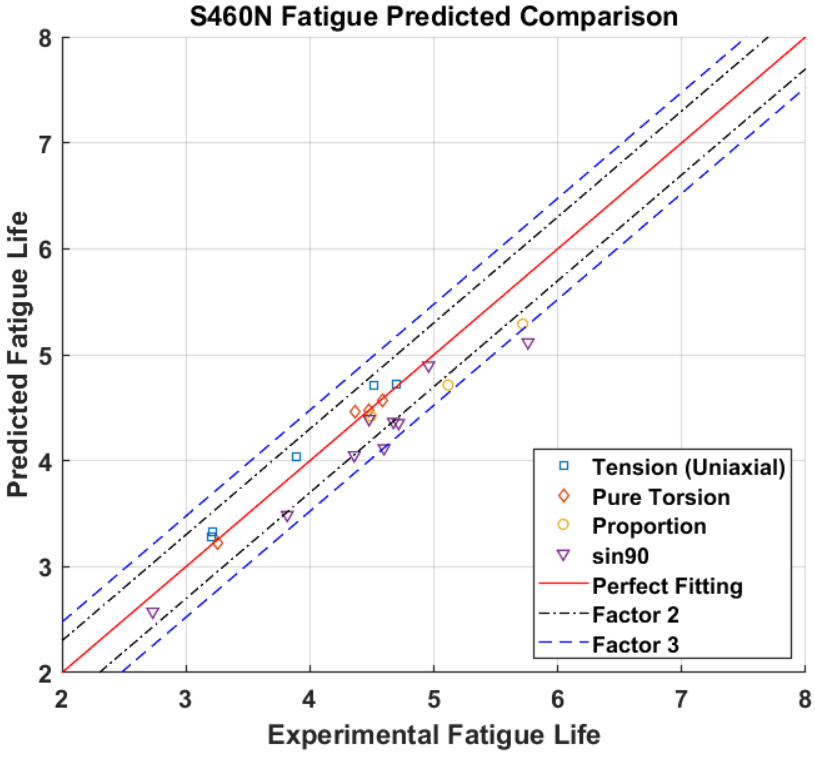

(e) S460N

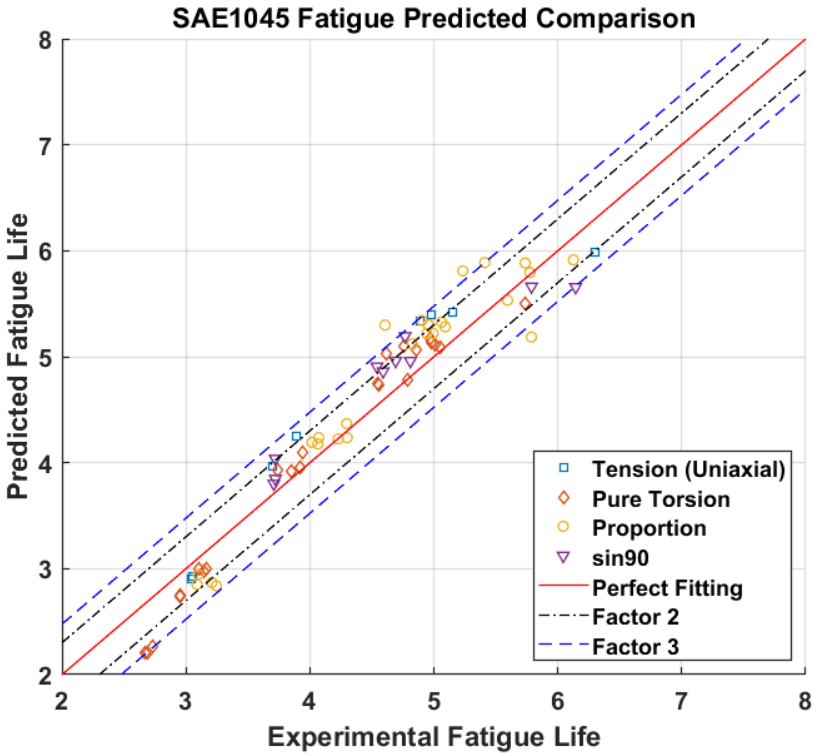

(d) SAE 1045

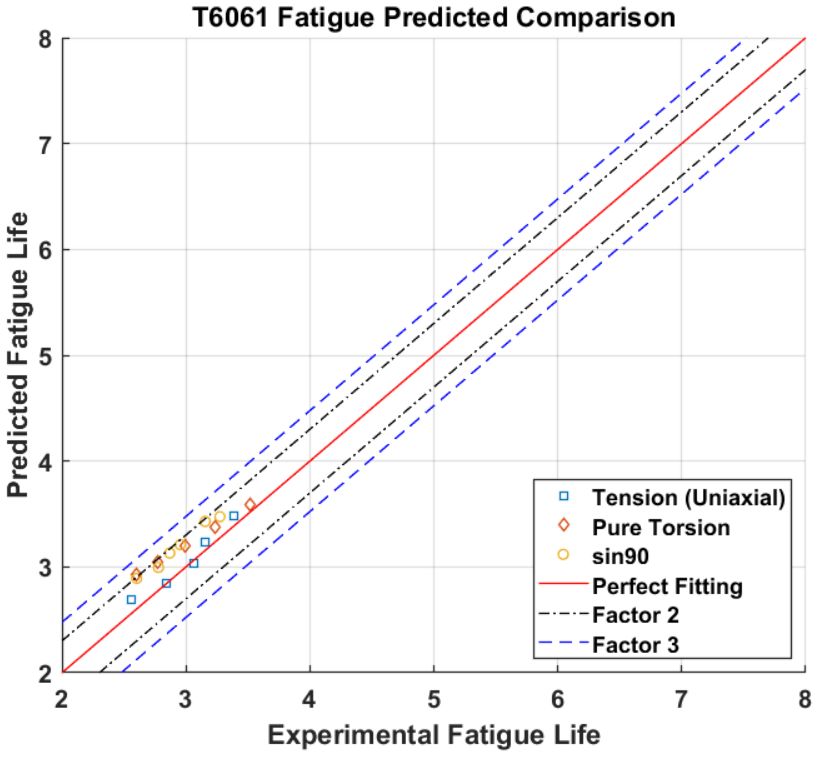

(f) Al T6061

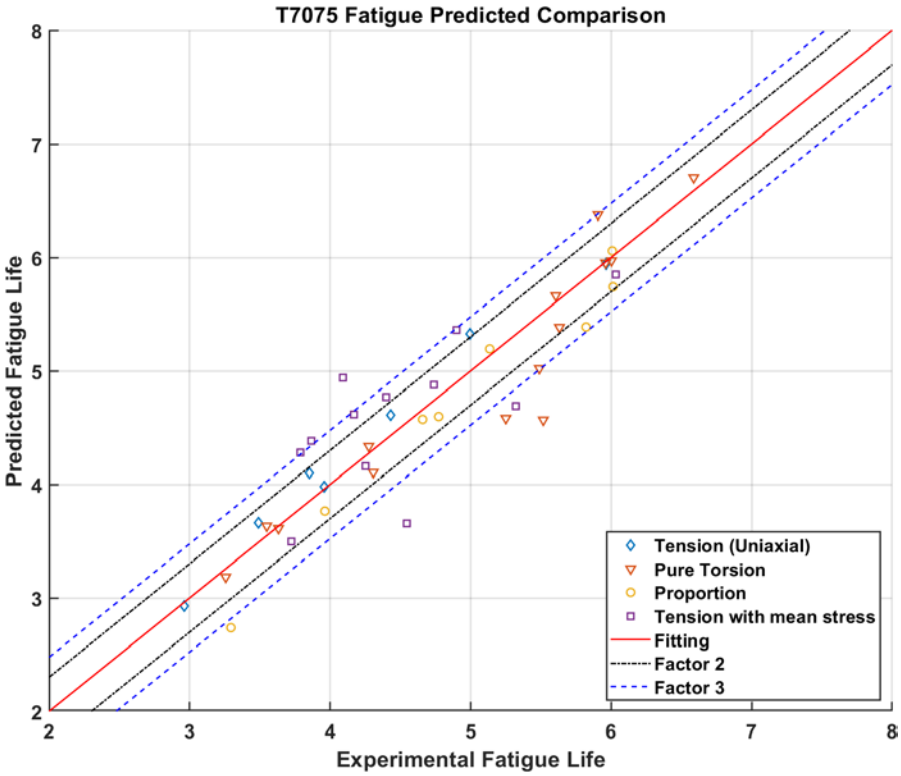

(g) Al T7075

Fig. 12 Predicted Fatigue Life and Experimental Fatigue Life Comparison in Constant Loading Case: (a) AISI 304 Steel (b) SM45C Steel (c) A533B (d) S460N (e) SAE 1045 (f) Al T6061 (g) Al T7075

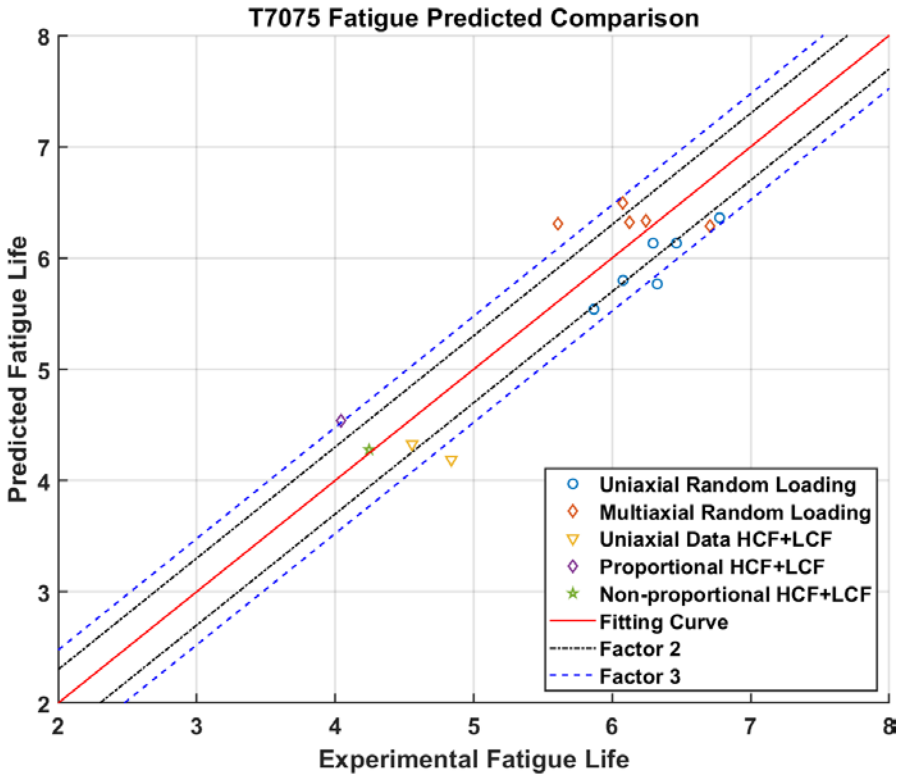

Fig. 13 Predicted Fatigue Life and Experimental Fatigue Life Comparison in Random Loading Case for Al T7075

The time-based model does not consider the frequency of the sampling rate of the datasets. Fig. 14 shows the predicted results at different sampling points. Note that the different sampling points could influence the deviation value of predicted fatigue life since the peak point and valley points in the spectrum could be missing when reducing the sampling points. For example, there are 517 points in every cycle under the original spectrum. The peak point could be missing when the sample points are reduced by every three points. However, even if the peak value and valley points are missing, the deviation values of the predicted fatigue life would show little difference and the result would be acceptable.

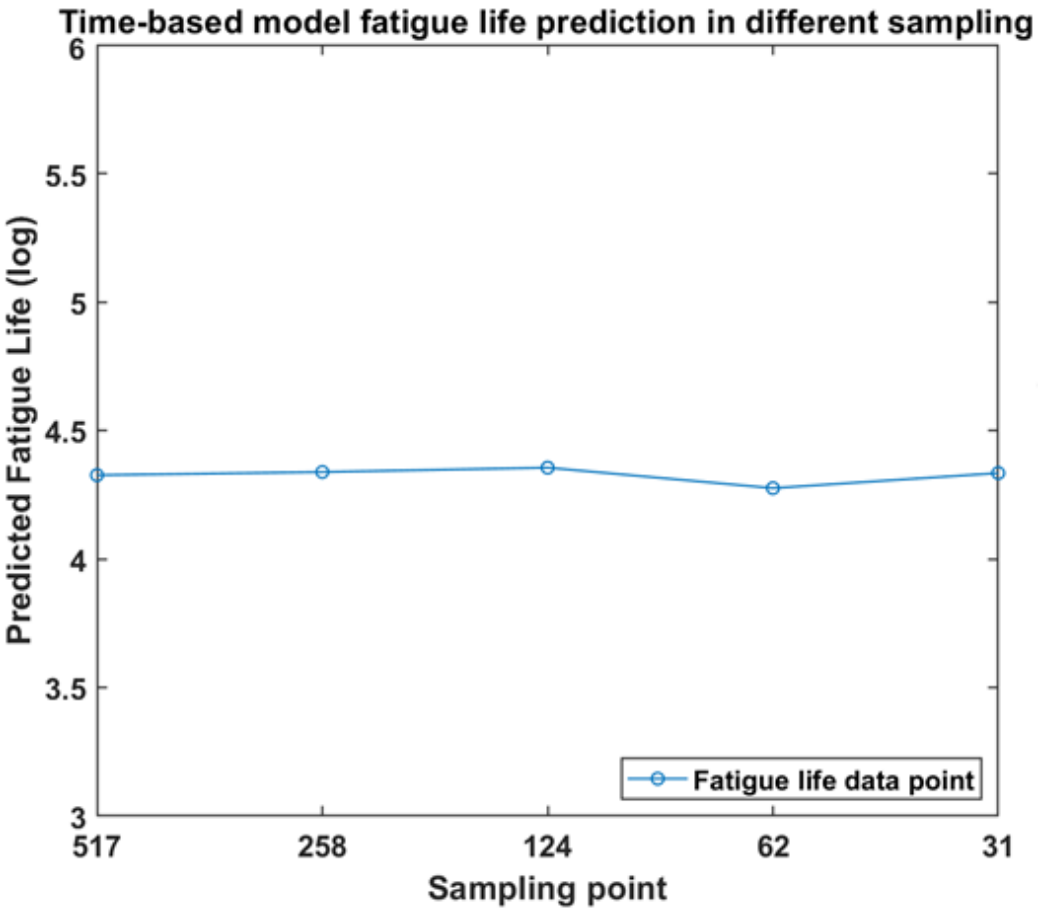

Fig. 14 The Predicted Fatigue Life in Different Sampling Rate

3.5 Conclusion and future work

A new time-based damage integration in the energy phase model is proposed. This model can deal with both constant loading and random loading cases as well as other complex form spectrums. The model uses the concept based on a new damage propagation method which is developed by modifying the crack propagation method. Furthermore, the model uses the time-based concept suitable to deal with models with various spectrums. The model is developed to overcome both HCF and LCF regions. Rather than applying the rainflow-counting algorithm and critical plane, this model avoids the complicated processes by using integration of uniaxial and multiaxial fatigue life directly. A big advantage of this model is that it can handle several conditions at the same time compared

to other models. The model was validated by several experimental data of seven materials under the open literature. The results show high accuracy of predictions for these different materials. The current validation not only includes the HCF and LCF predictions but also works for the HCF+LCF spectrums. For future work, the biaxial loading cases will be tested since this model is assumed to be suitable for both multiaxial and biaxial fatigue cases. Since the SIF is applied, the data from the notch specimen could also be predicted by modifying the equations.

CHAPTER 4

4 SUMMARY

Two energy-based fatigue life models based on different methods are proposed. Both energy-based models apply the equivalent energy concept in the preprocessing which converts the stress and strain spectrum to the equivalent energy spectrum. The equivalent energy concept can be used to simplify the multiaxial loading cases into equivalent uniaxial loading cases. In addition, the method can be used to deal with biaxial loading cases since it assumes that the loading is three-dimensional loading. The first energy-based model combines Miner's rule and the rainflow-counting algorithm in order to predict fatigue life under random loading cases. This method converts the various loading to equivalent constant loading by using the rainflow-counting algorithm and calculates fatigue life by implementing Miner's rule. Although this method provides an improvement over the original energy-based model, which cannot calculate fatigue life in random loading cases, the accuracy of the prediction is not ideal. Therefore, the second model, the time-based fatigue model using the energy-based method, is proposed. The time-based model is based on a new damage propagation rule which is a modification from Paris' law and a new time-based damage propagation function to calculate the fatigue life. The time-based model can directly predict fatigue life by integrating the energy history which obtains corresponding damage value. The model is validated by experimental data that include data on seven materials using both constant loading and random loading cases. The predicted results agree with the empirical fatigue life.

The following lists summarize the advantage of the new time-based model.

1. The proposed model predicts fatigue life for both uniaxial loading and multiaxial loading cases using the equivalent energy concept has been involved. Moreover, the biaxial loading cases can also be operated under the equivalent energy concept.

2. The time-based model is suitable for dealing with both the high cycle fatigue (HCF) and low cycle fatigue (LCF) regions applying the energy-based method.
3. Fatigue predictions under both the constant loading and random loading cases is applicable for the proposed model since the time-based method can deal with various spectrums. The time-based method calculates corresponding damage at every time point. The fatigue life can be predicted by the damage accumulation rule.
4. The proposed model replaces the rainflow-counting algorithm by directly integrating equivalent energy spectrums to calculate fatigue life.

In sum, the proposed model is a comprehensive method that can apply to several loading cases. The time integration technique curtails the complex processes and can predict fatigue life easily.

Note that the data under the biaxial loading cases will be validated in future studies. Through expanding the new damage propagation rule, which considers the geometric parameter in the equation, the fatigue data gathered from notch specimens can be predicted as well.

REFERENCES

[1] Lazzarin P, Susmel L. A stress-based method to predict lifetime under multiaxial fatigue loadings. Fatigue Fract Eng Mater Struct 2003;26:1171–87. https://doi.org/10.1046/j.1460-2695.2003.00723.x.

[2] Wei H, Carrion P, Chen J, Imanian A, Shamsaei N, Iyyer N, et al. Multiaxial high-cycle fatigue life prediction under random spectrum loadings. Int J Fatigue 2020;134:105462. https://doi.org/10.1016/j.ijfatigue.2019.105462.

[3] Golos KM, Debski DK, Debski MA. A stress-based fatigue criterion to assess high-cycle fatigue under in-phase multiaxial loading conditions. Theor Appl Fract Mech 2014;73:3–8. https://doi.org/10.1016/j.tafmec.2014.07.005.

[4] Liu Y, Mahadevan S. Strain-based multiaxial fatigue damage modelling. Fatigue Fract Eng Mater Struct 2005;28:1177–89. https://doi.org/10.1111/j.1460-2695.2005.00957.x.

[5] Remes H. Strain-based approach to fatigue crack initiation and propagation in welded steel joints with arbitrary notch shape. Int J Fatigue 2013;52:114–23. https://doi.org/10.1016/j.ijfatigue.2013.03.006.

[6] Correia JAFO, De Jesus AMP, Ribeiro AS, Fernandes AA. Strain-based approach for fatigue crack propagation simulation of the 6061-T651 aluminium alloy. Int J Mater Struct Integr 2017;11:1–15. https://doi.org/10.1504/IJMSI.2017.087336.

[7] Zhu SP, Huang HZ, He LP, Liu Y, Wang Z. A generalized energy-based fatigue-creep damage parameter for life prediction of turbine disk alloys. Eng Fract Mech 2012;90:89–100. https://doi.org/10.1016/j.engfracmech.2012.04.021.

[8] Letcher T, Shen MHH, Scott-Emuakpor O, George T, Cross C. An energy-based critical fatigue life prediction method for AL6061-T6. Fatigue Fract Eng Mater Struct 2012;35:861–70. https://doi.org/10.1111/j.1460-2695.2011.01669.x.

[9] Wei H, Liu Y. An energy-based model to assess multiaxial fatigue damage under tension-torsion and tension-tension loadings. Int J Fatigue 2020;141:105858. https://doi.org/10.1016/j.ijfatigue.2020.105858.

[10] Branco R, Costa JD, Borrego LP, Berto F, Razavi J, Macek W. Multiaxial fatigue life assessment in notched components based on the effective strain energy density. Procedia Struct Integr 2020;28:1808–15. https://doi.org/10.1016/j.prostr.2020.11.003.

[11] Kruch S, Prigent P, Chaboche JL. A fracture mechanics based fatigue-creep-environment crack growth model for high temperature. Int J Press Vessel Pip 1994;59:141–8. https://doi.org/10.1016/0308-0161(94)90149-X.

[12] Carpinteri A, Ronchei C, Scorza D, Vantadori S. Fracture mechanics based approach to fatigue analysis of welded joints. Eng Fail Anal 2015;49:67–78. https://doi.org/10.1016/j.engfailanal.2014.12.021.

[13] Cruces AS, Lopez-Crespo P, Moreno B, Antunes F V. Multiaxial fatigue life prediction on S355 structural and offshore steel using the SKS critical plane model. Metals (Basel) 2018;8. https://doi.org/10.3390/met8121060.

[14] Chen J, Imanian A, Wei H, Iyyer N, Liu Y. Piecewise stochastic rainflow counting for probabilistic linear and nonlinear damage accumulation considering loading and material uncertainties. Int J Fatigue 2020;140:105842. https://doi.org/10.1016/j.ijfatigue.2020.105842.

[15] Liu Y, Mahadevan S. Multiaxial high-cycle fatigue criterion and life prediction for metals. Int J Fatigue 2005;27:790–800. https://doi.org/10.1016/j.ijfatigue.2005.01.003.

[16] Gonçalves CA, Araújo JA, Mamiya EN. Multiaxial fatigue: A stress based criterion for hard metals. Int J Fatigue 2005;27:177–87. https://doi.org/10.1016/j.ijfatigue.2004.05.006.

[17] Ninic D. A stress-based multiaxial high-cycle fatigue damage criterion. Int J Fatigue 2006;28:103–13. https://doi.org/10.1016/j.ijfatigue.2005.04.014.

[18] Golos KM. Multiaxial fatigue criterion effect 1996;0161:263–6.

[19] Banvillet A, Palin-Luc T, Lasserre S. A volumetric energy based high cycle multiaxial fatigue citerion. Int J Fatigue 2003;25:755–69. https://doi.org/10.1016/S0142-1123(03)00048-3.

[20] Lu C, Melendez J, Martínez-Esnaola JM. Fatigue damage prediction in multiaxial loading using a new energy-based parameter. Int J Fatigue 2017;104:99–111. https://doi.org/10.1016/j.ijfatigue.2017.07.018.

[21] Mróz Z. On the description of anisotropic workhardening. J Mech Phys Solids 1967;15:163–75. https://doi.org/10.1016/0022-5096(67)90030-0.

[22] Garud YS. A new approach to the evaluation of fatigue under multiaxial loadings. J Eng Mater Technol Trans ASME 1981;103:118–25. https://doi.org/10.1115/1.3224982.

[23] Xiang Y, Lu Z, Liu Y. Crack growth-based fatigue life prediction using an equivalent initial flaw model. Part I: Uniaxial loading. Int J Fatigue 2010;32:341–9. https://doi.org/10.1016/j.ijfatigue.2009.07.011.

[24] Lu Z, Xiang Y, Liu Y. Crack growth-based fatigue-life prediction using an equivalent initial flaw model. Part II: Multiaxial loading. Int J Fatigue 2010;32:376–81. https://doi.org/10.1016/j.ijfatigue.2009.07.013.

[25] Carpinteri A, Spagnoli A, Vantadori S. A review of multiaxial fatigue criteria for random variable amplitude loads. Fatigue Fract Eng Mater Struct 2017;40:1007–36. https://doi.org/10.1111/ffe.12619.

[26] Liu Y, Venkatesan KR, Zhang W. Time-based subcycle formulation for fatigue crack growth under arbitrary random variable loadings. Eng Fract Mech

2017;182:1–18. https://doi.org/10.1016/j.engfracmech.2017.07.005.

[27] Venkatesan KR, Liu Y. Subcycle fatigue crack growth formulation under positive and negative stress ratios. Eng Fract Mech 2018;189:390–404. https://doi.org/10.1016/j.engfracmech.2017.11.029.

[28] Downing SD, Socie DF. Simple rainflow counting algorithms. Int J Fatigue 1982;4:31–40. https://doi.org/10.1016/0142-1123(82)90018-4.

[29] Rychlik I. A new definition of the rainflow cycle counting method. Int J Fatigue 1987;9:119–21. https://doi.org/10.1016/0142-1123(87)90054-5.

[30] Liu Y, Lu Z, Xu J. A simple analytical crack tip opening displacement approximation under random variable loadings. Int J Fract 2012;173:189–201. https://doi.org/10.1007/s10704-012-9682-6.

[31] Zhang W, Liu Y. Investigation of incremental fatigue crack growth mechanisms using in situ SEM testing. Int J Fatigue 2012;42:14–23. https://doi.org/10.1016/j.ijfatigue.2011.03.004.

[32] Zhang W, Liu Y. In situ SEM testing for crack closure investigation and virtual crack annealing model development. Int J Fatigue 2012;43:188–96. https://doi.org/10.1016/j.ijfatigue.2012.04.003.

[33] Socie DF. Multiaxial fatigue damage models 1987.

[34] Nelson D V., Rostami A. Biaxial fatigue of a533b pressure vessel steel. J Press Vessel Technol Trans ASME 1997;119:325–31. https://doi.org/10.1115/1.2842312.

[35] Kim KS, Park JC, Lee JW. Multiaxial fatigue under variable amplitude loads. J Eng Mater Technol Trans ASME 1999;121:286–93. https://doi.org/10.1115/1.2812377.

[36] Kurath P, Downing SD, Galliart DR. Summary of non-hardened notched shaft round robin program. Soc Automot Eng Inc, Multiaxial Fatigue Anal Exp 1989:13–31.

[37] Jiang Y, Hertel O, Vormwald M. An experimental evaluation of three critical plane multiaxial fatigue criteria. Int J Fatigue 2007;29:1490–502. https://doi.org/10.1016/j.ijfatigue.2006.10.028.

[38] Araghi M, Rokhgireh H, Nayebi A. Evaluation of fatigue damage model of CDM by different proportional and non-proportional strain controlled loading paths. Theor Appl Fract Mech 2018;98:104–11. https://doi.org/10.1016/j.tafmec.2018.09.019.

[39] Itoh T, Nakata T, Sakane M, Ohnami M. Nonproportional low cycle fatigue of 6061aluminum alloy under 14 strain paths. vol. 25. Elsevier Masson SAS; 1999. https://doi.org/10.1016/S1566-1369(99)80006-5.

[40] Zhao T, Jiang Y. Fatigue of 7075-T651 aluminum alloy. Int J Fatigue 2008;30:834–49. https://doi.org/10.1016/j.ijfatigue.2007.07.005.

APPENDIX A

SPECTRUM TRANSFER

```
clc,clear all, close all
%% Material Properties
MP = xlsread('material properties.xlsx',7);
E = MP(1,1);
G = MP(2,1);
sig_y = MP(3,1);
Poisson = MP(4,1);
D0 = 0;
beta = 30.091 * sig_y^ -0.797;

a_ten = MP(5,1);
b_ten = MP(6,1);
a_tor = MP(7,1);
b_tor = MP(8,1);
% a_ten = MP(9,1);
% b_ten = MP(10,1);
ten_1 = a_ten * 4^b_ten;
tor_1 = a_tor * 4^b_tor;
s = ten_1 / tor_1;

%% Data input [HCF]
% strain_stress = xlsread('loading_dataset.xlsx',1); % Constant loading
% strain_stress =
importdata('Non_Proportional_FALLSTAFF_f2500L_edited_cwt.txt'); % Random
loading
```

```
if length(strain_stress(1,:)) == 4
   strain_stress = strain_stress;
elseif length(strain_stress(1,:)) == 1
   stress = strain_stress;
   strain = strain_stress ./ E;
   strain_stress = [strain stress zeros(length(strain_stress(:,1)))
zeros(length(strain_stress(:,1)))];
elseif length(strain_stress(1,:)) == 2
   stress = strain_stress(:,1);
   shear_stress = strain_stress(:,2);
   ep = stress ./ E;
   gama = shear_stress ./ G;
   strain_stress = [ep stress gama shear_stress];
else
   strain_stress = strain_stress(:,1) == [];
   stress = strain_stress;
   strain = strain_stress ./ E;
   strain_stress = [strain stress zeros(length(strain_stress(:,1)))
zeros(length(strain_stress(:,1)))];
end

%% Data input [LCF]
% strain_stress = xlsread('Multi_HC_pro.xlsx'); % multi HCF LCF pro data
% strain_stress = xlsread('Multi_HC_nonpro.xlsx'); % multi HCF LCF nonpro data
strain_stress = load('strain_stress_NN_original_modified.mat');
```

```
% strain_stress = load('strain_stress_linear_original_modified.mat');
strain_stress = strain_stress.strain_stress;
% strain_stress(:,1) .* 2;
% strain_stress = [ans strain_stress(:,2) zeros(length(strain_stress),1)
zeros(length(strain_stress),1)];
%% Convert the spectrum to equivalent energy
U_eqv = [];
[U_dis_spec, U_dil_spec] = Energy_test(strain_stress);
for i = 1:length(strain_stress(:,1))
[U_eqv(i)] = Fatigue_Model_D(ten_1, tor_1, Poisson, a_ten, b_ten, U_dis_spec(i),
U_dil_spec(i));
end
U_eqv = U_eqv';
```

APPENDIX B

TIME-BASED FATIGUE MODEL FOR CONSTANT LOADING CASE

```
clear all, clc
% Given
MP = xlsread('material properties.xlsx',7);
E = MP(1,1);
G = MP(2,1);
sig_y = MP(3,1);
Poisson = MP(4,1);
D0 = 10^-2.5;
beta = 30.091 * sig_y^ -0.797;

% a_ten = MP(5,1);
% b_ten = MP(6,1);
% a_tor = MP(7,1);
% b_tor = MP(8,1);

a_ten = MP(9,1);
b_ten = MP(10,1);
d_ten = 0.01;

%% %%%%%%%%%%%%%%%%%%%% DATA
%%%%%%%%%%%%%%%%%%%%%%%%
N_life = [];
T_D = [];
collect_A = [];
Load = load('loading_data_7075.mat');
```

```
% ten_mean = load('testmid.mat');
Load = Load.U_eqv;
for k = 1:length(Load)
   Load1 = [0;Load(k)];
   for j = 1:25
      Load1 = [Load1;Load1];
   end
U_T = Load1;

%% Fatigue Model
i = 1;
D = 10^-2.5;
R_ten = 0.; % R ratio
m_ten = -2 / b_ten;
C_ten = (2 * a_ten * E * pi)^(-m_ten/2) * 2 *(1-D0^((2-m_ten)/2))/(2-m_ten);
B_ten = m_ten - 2 * d_ten;
A_ten = C_ten * (1-R_ten)^B_ten * (2*E*sig_y)^d_ten / 0.36^d_ten; % R>0

while D < 1
   if U_T(i) < U_T(i+1)
      Umax = max(U_T(i:100+i)); % from Kmax

%       A_ten = C_ten * sqrt(2*E_7075 *sig_y) * (1-R_ten)^(B_ten) * (1 - beta *
R_ten)^(-2 * d_ten)/0.6;
      alf_ten = A_ten * (2 * E * Umax * pi)^(B_ten/2) * (pi / sig_y)^(d_ten);
```

```
        eqU = (U_T(i+1)^(d_ten) - U_T(i)^(d_ten));
        dD_dn = alf_ten * eqU * D^((B_ten/2)+d_ten);
    else
        dD_dn = 0;
    end
    delta_a = (U_T(i) * pi * D /sig_y);
    D = dD_dn + D;
    D_his(i) = D;
    delta(i) = delta_a;
    i = i+1;
end
    %% Life
    N_life(k) = log10(i/2)
end
N_life = N_life';


p = N_life;
e = [2.962369336
3.48756256
3.853941446
3.959613711
4.431540663
4.996892388
5.963640048
```

% % tor

3.256958153

3.54863506

3.632558515

4.275126999

4.306875174

5.250578564

5.488753716

5.516952942

5.606092097

5.631960961

5.906218101

5.960729945

6.002244271

6.587445819

% pro

3.29380436

3.962558736

4.772277688

5.135596923

4.658011397

5.821269128

6.007747778

6.013338693]';

%ten with mean stress

```
% 3.722222464
% 3.788451207
% 4.089481203
% 4.252488944
% 4.543521731
% 4.737828506
% 5.320638485
% 6.031758587
% 4.899404606
% 3.86421433
% 4.169733198
% 4.397575048]';

a = [2,8];
b = [2,8];

% Plot Chart
figure
hold on
grid on
plot(e(1:7), p(1:7),'p')
plot(e(8:21), p(8:21),'v')
plot(e(22:29), p(22:29),'d')
% plot(e(30:41), p(30:41),'s')
% plot(e(1:15), p(1:15),'o')
```

```
plot(a,b,'red')
collect_A = [2+log10(2),8];
d = [2,8-log10(2)];
plot(collect_A,d,'Color','black','LineStyle','-.')
collect_A = [2+log10(3),8];
d = [2,8-log10(3)];
plot(collect_A,d,'Color','blue','LineStyle','--')

e = [2,8-log10(2)];
f = [2+log10(2),8];
plot(e,f,'Color','black','LineStyle','-.')

e = [2,8-log10(3)];
f = [2+log10(3),8];
plot(e,f,'Color','blue','LineStyle','--')

xlabel('Experimental Fatigue Life')
ylabel('Predicted Fatigue Life')
legend('Tension (Uniaxial)','Pure Torsion','Proportion','Perfect Fitting','Factor 2','Factor
3','Location','southeast')
% title('(Energy)Time-Based Fatigue Predicted Comparison')
title('T7075 Fatigue Predicted Comparison')
```

APPENDIX C

TIME-BASED FATIGUE MODEL FOR RANDOM LOADING CASE

```
clear all, clc, close all
%%
% Material Parameters
E_7075 = 71700;
G_7075 = 26900;
sig_y = 503;
sig_u = 570;
Poisson = 0.306;
D0 = 10^-2.5;
D = 10^-2.5;
beta = 30.091 * sig_y^ -0.797;
d_ten = 0.01;
% Energy fitting data from paper
a_ten = 9.4994;
b_ten = -0.263;

%% Data input

% Load = load('con_1_try_0302.mat')
Load = load('test1_u1.mat') % 6.3606
% Load = load('test1_u2.mat') % 6.1327
% Load = load('test1_u3.mat') % 6.1335
% Load = load('test1_u4.mat') % 5.7669
% Load = load('test1_u5.mat') % 5.7666
% Load = load('test1_u6.mat') % 5.5383
```

```
% Load = load('test1_p1.mat') % 6.3175
% Load = load('test1_p2.mat') % 6.3349
% Load = load('test1_p3.mat') % 6.2877
% Load = load('test1_np1.mat') % 6.4983
% Load = load('test1_np2.mat') % 6.3102

% Load = load('LL_0228_2.mat') % 5481914
% Load = load('NN_0228_2.mat') % 4920102
% Load = load('LL_0228.mat') % 78546809
% Load = load('NN_0228.mat') % 36770215

% Load = load('pro_m_0226.mat') %2.7332
% Load = load('non_m_0226.mat') %3.0730

% Load = load('test_mpro_0304.mat') %4.1868
% Load = load('test_mnonpro_0304.mat') %4.3260
% Load = load('test_u_linear_0304.mat') %35790655 4.5393
% Load = load('test_u_nonlinear_0304.mat') %19566025 4.2770

Load = Load.U_eqv;

Load = [Load;Load;Load;Load;Load;Load;Load;Load];
% Load = [Load;Load;Load;Load;Load;Load;Load;Load];
% Load = [Load;Load;Load;Load;Load;Load;Load;Load];
```

```
% Load = [Load;Load;Load;Load;Load;Load;Load;Load];
% Load = [Load;Load;Load;Load;Load;Load;Load;Load];
U_T = Load;

%% Find A and B fitting parameters
R_ten = 0.; % R ratio
m_ten = -2 / b_ten;
C_ten = (2 * a_ten * E_7075 * pi)^(-m_ten/2) * 2 *(1-D0^((2-m_ten)/2))/(2-m_ten);
B_ten = m_ten - 2 * d_ten;
A_ten = C_ten * (1-R_ten)^B_ten * (2*E_7075*sig_y)^d_ten / 0.36^d_ten;

%% Fatigue Model
i = 1;
while D < 1
  if U_T(i) < U_T(i+1)
    Umax = max(U_T(i:100+i)); % from Kmax
    alf_ten = A_ten * (2 * E_7075 * Umax * pi)^(B_ten/2) * (pi / sig_y)^(d_ten);
    eqU = (U_T(i+1)^(d_ten) - U_T(i)^(d_ten));
    dD_dn = alf_ten * eqU * D^((B_ten/2)+d_ten);
  else
    dD_dn = 0;
  end
  D = dD_dn + D;
  D_his(i) = D;
  i = i+1;
```

```
end
%% Plot the D-N curve
% x = 1:i-1;
% y = D_his;
% plot(x,y)
% grid on
% xlabel('Life (N)')
% ylabel('Damage (D)')
% legend('Trend')
%% Fatigue life in log scale
N_life = log10(i)
```